The Role of Contact Angle and Pore Width on Pore Condensation and Freezing

Robert O. David[1,a], Jonas Fahrni[2,b], Claudia Marcolli[1], Fabian Mahrt[1], Dominik Brühwiler[2], and Zamin A. Kanji[1]

[1]Institute for Atmospheric and Climate Science, ETH Zürich, 8092 Zürich, Switzerland
[2]Institute of Chemistry and Biotechnology, Zürich University of Applied Sciences (ZHAW), 8820 Wädenswil, Switzerland

[a]Now at Department of Geosciences, University of Oslo, Oslo, 0315, Norway
[b]Now at RISE Processum AB, Bioeconomy and Health, Örnsköldsvik, SE-891 22, Sweden

Correspondence to: Robert O. David (r.o.david@geo.uio.no) or Zamin A. Kanji (zamin.kanji@env.ethz.ch)

Abstract. It has recently been shown that pore condensation and freezing (PCF) is a mechanism responsible for ice formation under cirrus cloud conditions. PCF is defined as the condensation of liquid water in narrow capillaries below water saturation due to the inverse Kelvin effect, followed by either heterogeneous or homogeneous nucleation depending on the temperature regime and presence of an ice nucleating active site. By using sol-gel synthesized silica with well-defined pore diameters, morphology and distinct chemical surface-functionalization, the role of the water-silica contact angle and pore width on PCF is investigated. We find that ~~fcontact angle and pore width play an important role in determining the relative humidity required for capillary condensation as predicted by the Kelvin effect and subsequent ice nucleation at cirrus temperatures. F~~or the pore diameters and water contact angles covered in this study, 2.2 – 9.2 nm and 15 – 78˚, respectively, our results reveal that the water contact angle plays an important role in predicting the humidity required for pore filling while the pore diameter determines the ability of pore water to freeze. For T > 235 K and below water saturation, pore diameters and water contact angles were not able to predict the freezing ability of the particles suggesting an absence of active sites, thus ice nucleation did not proceed via a PCF mechanism. Rather, the ice nucleating ability of the particles depended solely on chemical functionalization. Therefore, parameterizations for the ice nucleating abilities of particles at cirrus conditions should differ from parameterizations at mixed-phase clouds conditions. Our results support PCF as the atmospherically relevant ice nucleation mechanism below water saturation when porous surfaces are encountered in the troposphere.

1 Introduction

In the Earth's atmosphere, ice crystals are important for precipitation formation (Mülmenstädt et al., 2015), cloud lifetime, radiative properties, and ultimately modulate climate (McFarquhar et al., 2017; Seinfeld et al., 2016). Understanding the formation of ice crystals is therefore essential to accurately predict cloud properties and thus future climate. The freezing temperature of pure water droplets is approximately 235 K, known as the homogeneous freezing temperature (HFT). However, ice formation is also observed at temperature ~~(~~T~~)~~ > HFT or below water saturation. At T > HFT ice formation takes place

heterogeneously and is ~~initiated~~ aided by the presence of a ~~so-called ice active site~~foreign substance (Fletcher, 1969; Kaufmann et al., 2017; Kiselev et al., 2017; Vali et al., 2015), which lowers the energy barrier required for the homogeneous nucleation of ice. Below water saturation, ice nucleation is conventionally defined as deposition nucleation, or the direct transition from water vapour to the ice phase without an intermediate liquid water phase (Pruppacher and Klett, 1997; Vali et al., 2015). However, it has been shown that ice nucleation below water saturation occurs in the presence of cracks and steps (Campbell et al., 2017; Christenson, 2013; David et al., 2019; Fukuta, 1966; Higuchi and Fukuta, 1966; Kovács et al., 2012; Kovács and Christenson, 2012; Pach and Verdaguer, 2019; Wang et al., 2016) and has subsequently been termed pore condensation and freezing (PCF) (Campbell and Christenson, 2018; David et al., 2019; Marcolli, 2014; Pach and Verdaguer, 2019; Umo et al., 2019; Vali et al., 2015; Wagner et al., 2016). PCF occurs when liquid water, which can exist in narrow pores, cracks, cavities or capillaries (hereafter referred to as pores) below ambient water saturation, freezes~~PCF occurs when bulk water, which can exist below water saturation in narrow pores, cracks, cavities or capillaries (hereafter referred to as pores) freezes~~. Due to the negative or concave curvature of water in confinements, the vapour pressure required for condensation to occur in a pore compared to a flat/bulk water surface can be predicted by the inverse version of the Kelvin equation given as:

$$\frac{p_{lc}}{p_l} = \boldsymbol{exp}\left[\frac{-4\gamma(T)v_l(T)}{\frac{D}{\cos\theta}RT}\right], \quad (1)$$

where p_{lc} is the vapor pressure of water over a concave surface, p_l is the vapor pressure of water over a flat surface, and $\frac{p_{lc}}{p_l}$ denotes the saturation ratio w.r.t water, while $\gamma(T)$ is the temperature dependent surface tension of the water-vapour interface, $v_l(T)$ is the molar volume of water as a function of temperature, D is the pore diameter, R is the gas constant and T is the temperature in Kelvin. θ is the contact angle of water on the (pore) material or the wettability of the material, where $\theta = 0°$ ($\cos\theta = 1$) denotes a perfectly wettable surface, whereas higher water contact angles denote less hydrophilic surfaces (Lohmann et al., 2016). As deduced from Eq. 1, the relative humidity w.r.t. water (RH_w) required for a pore to fill depends on the pore diameter and the water contact angle of the pore surface. As such, at a given water contact angle a narrower pore will fill at a lower RH_w than a wider pore. Conversely, for a fixed pore diameter, the higher the contact angle of water on the pore surface, the higher the RH_w required for pore filling.

Once the pore is filled, the water can freeze either homogeneously or heterogeneously depending on the temperature regime or the presence of an ice active site, as long as the pore is wide enough to host the critical ice germ (Campbell et al., 2017; Campbell and Christenson, 2018; David et al., 2019; Koop, 2017; Marcolli, 2014). In order for the phase transition from supercooled water to ice to occur, Classical Nucleation Theory predicts that a large enough cluster of water molecules, known as a germ, must organize into ice before the entire water volume can freeze (Fletcher, 1962; Lohmann et al., 2016; Pruppacher and Klett, 1997). The radius of this critical ice germ (r_c) can be calculated as:

$$r_c = \frac{2\sigma_{iw}v_{ice}}{RTln\frac{p_w}{p_i}(S_i)}, \quad (2)$$

where σ_{iw} is the interfacial energy between the ice and water interface, v_{ice} is the approximate volume of bulk ice, and $\frac{p_w}{p_i}$~~S_t~~ is the ratios of the equilibrium vapour pressures over water and ice~~supersaturation with respect to ice~~. Additionally, it has been shown that even down to extreme supercooling (T < 200 K), a quasi-liquid layer of water is present along the pore wall (Jähnert et al., 2008; Marcolli, 2014; Moore et al., 2010; Schreiber et al., 2001). The width of the quasi-liquid layer has been shown to depend on temperature and surface chemistry but the exact thickness of the layer varies greatly between different observational techniques and MD studies (Bartels-Rausch et al., 2014). Nevertheless, the thickness of the quasi-liquid layer can be parameterized by fitting the measured melting point depressions of ice in pores to a modified version of the Gibbs-Thomson equation and has been shown to vary between 1 and 2 monolayers thick for the pore diameters and across the temperature range investigated in this study (Findenegg et al., 2008; Jähnert et al., 2008; Marcolli, 2014; Schreiber et al., 2001; Wang et al., 2019). When accounting for the quasi-liquid layer thickness, assumed as t = 0.38 nm (Schreiber et al., 2001), ~~Thus,~~ the diameter of a pore capable of hosting ice (D_p) can be expressed as:

$$\boldsymbol{D_p \geq 2r_c + 2t}\text{~~,~~} \quad (3)$$

~~where t is the thickness of the quasi liquid layer, assumed as t = 0.38 nm (Schreiber et al., 2001).~~ Indeed, Marcolli (2014) reported that D_p is a good predictor for ice forming in porous silica particles. However, once pore ice is formed, it must grow out of the pore, i.e. into the unconfined vapour region. Based on CNT, the ice growing out of the pore needs to be supercritical ~~e~~with respect to the vapour phase. The energy barrier for nucleation in the vapour phase is significantly higher than that in water.~~nergy cost for ice growth into the vapour phase is more expensive than for growth within water.~~ This increase in energy barrier~~d cost~~ comes from the need to replace~~,~~ σ_{iw} with the interfacial energy between ice and vapour (σ_{iv}) in Eq. 2, which is approximately a factor of 4.8 larger than σ_{iw} at 236 K (Cooper, 1974; Ickes et al., 2015; Ketcham and Hobbs, 1969). Additionally, as the ice growing out of the pore experiences an environment that is subsaturated with respect to water, ~~the ice forming in a pore experiences water saturation and therefore the~~ $\frac{p_w}{p_i}$~~S_t~~ in Eq. 2 must be replaced by the ice saturation ratio (S_i), which is smaller than $\frac{p_w}{p_i}$~~is higher than the S_t outside of the pore~~. Therefore, the critical radius for ice growth out of the pore is much larger than that of the critical radius in the pore necessitating a substantial increase in S_i for ice to be able to grow out of a pore (David et al., 2019; Koop, 2017). Indeed, Campbell et al~~.~~ (2017) and Campbell and Christenson (2018), showed that an increase in supersaturation is required for crystallites formed in wedge shaped pores to emerge into the unconfined vapour region, which they interpreted as a second energy barrier for ice growth out of pores. In addition, molecular dynamic simulations (MDS) conducted by Page and Sear (2006) showed that protein crystal nucleation out of single pores is maximized when the pore width is close to the critical nucleus size in order to minimize the energy for pore filling and for the crystal growth out of the pore. Conversely, mesoporous silica with closely spaced cylindrical pores did not reveal any inhibition of ice growth out of pores (David et al., 2019). This result is supported through MDS and CNT based calculations revealing that an arrangement of several subcritical cylindrical pores closely spaced together greatly decreases S_i required for ice growth out of pores due to pore-ice bridging across adjacent pores (David et al., 2019).

Although there is strong evidence that pores are responsible for ice nucleation below water saturation, the ability of PCF to predict ice nucleation as a function of pore width and water contact angle has not been shown systematically. For example, in an earlier study we showed that pores were responsible for the observed ice nucleation of synthesized silica and NX-illite particles and that the humidities required for ice formation were consistent with PCF (David et al., 2019). Here we present results from synthesized porous silica with well-defined pore diameters, geometry, and water contact angles to better understand the PCF mechanism and its predictive capability for ice nucleation at water subsaturated conditions.

2. Methods

2.1 Particle synthesis

2.1.1 Synthesis of MCM-41 submicron mesoporous silica particles

The MCM-41 (see Fig. 1a and b) particles were synthesized ~~F~~following Beck et al., (1992), NH_4OH (121 mL, 28 %, Sigma-Aldrich)~~:~~, deionized water (300 mL) and ethanol (500 mL, 99.8 %, Sigma-Aldrich) were stirred for 5 min in a 1 L polypropylene beaker. For the synthesis of materials with 2.8 nm or 3.3 nm pores, C_{16}TMABr (hexadecyltrimethylammonium bromide, 1.74 g, 99 %, Acros) was subsequently added and stirred for 15 min before TEOS (tetraethoxysilane, 4.5 mL, 20.2 mmol, 98 %, Sigma-Aldrich) was quickly dropped into the reaction mixture. For 2.5 nm pores, a mixture of C_{16}TMABr (0.871 g, 99 %) and C_{14}TMABr (tetradecyltrimethylammonium bromide, 0.804 g, 99 %, Sigma-Aldrich) was used. After a few minutes, silica started to precipitate. The reaction was stirred at room temperature for 2 h before filtering (Sartorius® 393). The filter cake was subsequently washed twice with 50 mL of deionized water, dried at T = 80 ˚C for approximately 1 h and finally ground in methanol for 3 min. To obtain 3.3 nm pores, the dried particles were transferred into a Teflon lined acid digestion vessel~~bomb~~ (Parr 4748), suspended in deionized water (80 mL), aged (80 °C , 24 h), subsequently filtered (Sartorius® 393), dried, and ground in methanol (99 %, Sigma-Aldrich). After drying again (80 ˚C, ≥ 1 h), the particles were calcined at 550 ˚C for 12 h.

2.1.2 Synthesis of SBA-15 submicron mesoporous silica particles

To obtain larger pore diameters (~ 9 nm), SBA-15 particles (see Fig. 1c and d) were synthesized ~~S~~similarly to Linton et al.~~,~~ (2009b) where Pluronic® P104 (1.25 g, BASF) was dissolved under vigorous stirring in a hydrochloric acid solution (200 mL, 1.6 mol·L^{-1}) at 60 ˚C and TMOS (tetramethoxysilane, 8 mL, 99 %, Sigma-Aldrich) was added quickly under vigorous stirring. After 1 min (approximate hydrolysis time, Linton et al., 2009a) the stirring rate was lowered to moderate stirring. After another 1 min, the reaction mixture was diluted with a hydrochloric acid solution (200 mL, 1.6 mol·L^{-1}) leading to precipitation of the silica. The reaction mixture was further stirred at 60 °C for 24 h. The resulting suspension was centrifuged, washed with deionized water (200 mL) twice, and the product was transferred to ~~a~~the ~~Teflon~~ Teflon ~~bomb~~lined acid digestion vessel. The

wet particles were dispersed in deionized water (60 mL) and the pH was adjusted to 9 by the addition of NH_4OH (1.05 mL, 28 %). The mixture was aged in quiescent conditions at 80 ˚C for 15 h. The suspension was centrifuged and washed with deionized water (200 mL) twice and once with ethanol (70 %). The white powder was dried (80 °C, ≥ 1 h) before it was ground in methanol (99 %) for 3 min. After drying again (80 ˚C, ≥ 1 h), the particles were calcined at 550 ˚C for 12 h.

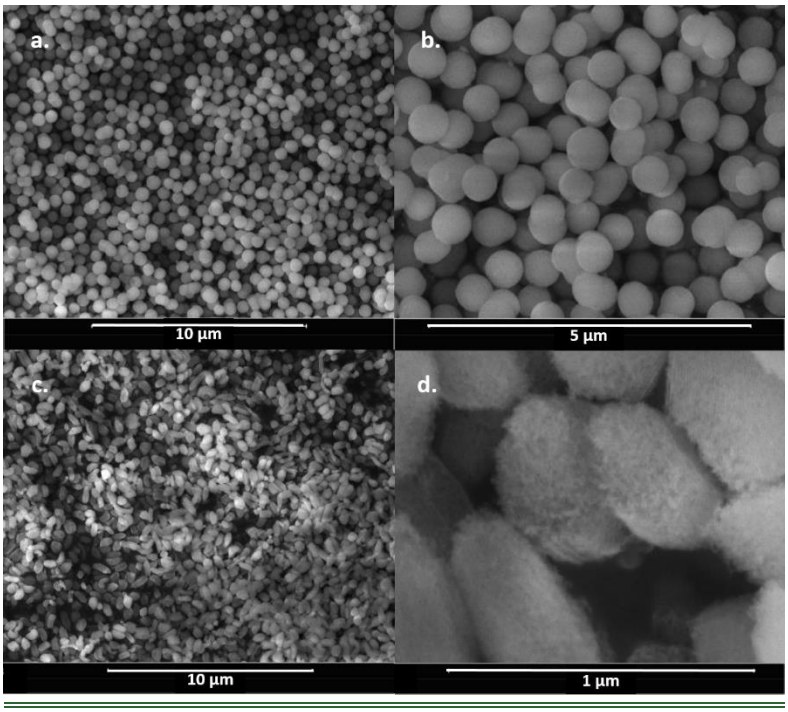

Figure 1: Scanning election microscopy images of 2.8H2 (a. and b.) as an example of MCM-41 particles and 9.0M2 (c. and d.) as an example of SBA-15 particles.

2.1.3 Particle functionalization

In order to investigate the impact of water contact angle on the ability of porous particles to nucleate ice via PCF, particles of similar pore diameters were functionalized with trimethyl and hydroxyl groups after calcination. We will focus on ice nucleation experiments with ~~–~~particles functionalized with trimethyl and hydroxyl groups rather than just calcined ones, ~~because these were observed to change~~as their water contact angle was observed to change with ageing in air (Muster et al., 2001). ~~-~~A batch of 2.8 nm pore samples was calcined at 550 ˚C and then separated into three parts with one part unmodified, one part hydroxylated and the remaining part methylated. A summary of the particles investigated in this study is provided in Table 1. Hydroxylation and methylation were conducted as follows:

Silanol surface (hydroxylation): A calcined sample (1.0 g) was suspended in toluene (200 mL) and heated to 60 °C before a calculated amount of water was added (Eq. A1 of Appendix A1) in order to achieve a concentration of 4.6 silanol groups nm^{-2}

(Zhuravlev, 2000). The particles were then suspended for 60 minutes through vigorous stirring, and occasional sonication, before ~~they were filtered off~~the suspension was filtered and ~~,~~ washed with deionized water (80 mL) and dried (120 °C, 20 mbar) overnight.

Alkyl surface (trimethylation): A calcined sample (1.0 g) was suspended in toluene (200 mL at 60 ˚C) before a 2-fold excess of organosilane (trimethylchlorosilane, 99 %, Sigma-Aldrich) as calculated using Eq. A2 (Appendix A1) was added. The reaction was run for 3 h and then the suspension was filtered and washed with toluene (50 mL), ethanol (50 mL), and water (50 mL). The particles were then dried (120 °C, 20 mbar) overnight.

2.2 Particle characterization

2.2.1 Nitrogen adsorption and calculation of pore size distribution

Particle surface area (S_{BET}) and pore diameters were determined by nitrogen adsorption (Quantachrome, NOVA 3000e). The nitrogen isotherms were obtained by measuring > 10 m^2 of dried (80 ˚C) sample and the S_{BET} was obtained from the relative pressure range where multilayer adsorption takes place (0.05-0.30) and applying the Brunauer, Emmett and Teller (BET) gas adsorption ~~equation~~theory (Brunauer et al., 1938). The average pore diameter (d_{DFT}) was obtained using the NLDFT (non-local density functional theory) method (Landers et al., 2013) applied to the N_2 sorption measurements.

2.2.2 DRIFTS

Diffuse reflectance infrared Fourier transform spectroscopy (DRIFTS) was used to characterise the functionalised particles and estimate the concentration of hydroxyl and methyl groups on the silica particles. The samples were prepared by combining 6 mg of dried sample (80 ˚C, > 1 h) with 194 mg of dry potassium bromide (KBr) to produce a 3 % (w/w) mixture. The mixture was ground vigorously for over a minute (Hamadeh et al., 1984) before being filled in the sample holder, where the sample was flattened with a spatula. A scan resolution of 4 cm^{-1} was chosen and background scans with pure KBr were performed and each sample was corrected accordingly. The mixtures were scanned immediately after grinding to avoid the adsorption of water vapour. The background corrected scans were averaged and then normalized to the BET surface area of the sample instead of using the traditional method of normalizing based on the Si-O asymmetric stretching peak in the vicinity of 1100 cm^{-1} (Muster et al., 2001). Normalization to the BET surface is more appropriate considering the porous nature of the samples.

2.2.3 Water sorption and water contact angle derivation

Water sorption isotherms were obtained using dynamic vapour sorption (DVS, TA Instruments, VTI-SA+), where the water uptake is determined gravimetrically. Each isotherm was obtained using approximately 10 mg of sample dried at 120 ˚C in a pure nitrogen atmosphere for 1 h before the reference mass was determined in order to evaporate any pre-adsorbed water. The DVS cell was then cooled to the temperature (T = 25 ˚C), at which the sorption measurements were performed. The adsorption

isotherms were obtained by continuously measuring the sample mass while increasing the humidity from 0 to 90 % in steps of 5 % RH_w. The water uptake reported here denotes quasi equilibrium values at each RH_w step defined as a mass change rate less than 0.008 % over the course of 5 min. The water contact angle of the sample surface was then determined from the sorption isotherm using the Cohan-Kelvin equation (Kocherbitov and Alfredsson, 2007):

$$\boldsymbol{r_{nldft} - t_{ads} = -\frac{2\gamma(T)\cos(\theta)v_l(T)}{RTln(p/p_0)}}. \quad (4)$$

Here t_{ads} is the statistical thickness of adsorbed water, r_{nldft} is the pore radius as determined by NLDFT ($d_{DFT}/2$) and p/p_0 is the water saturation ratio or $RH_w/100$. The statistical thickness in cylindrical pores is calculated by subtracting the volume of the adsorbate (V_{ads}) from the full pore volume (V_{tot}) and can be rewritten as:

$$\boldsymbol{r_{nldft} - t_{ads} = \frac{r_{nldft}}{\sqrt{\frac{V_{tot}}{V_{tot}-V_{ads}}}}}, \quad (5)$$

By substituting Eq. 5 into Eq. 4, the Cohan-Kelvin equation for cylindrical pores can be written as:

$$\boldsymbol{r_{nldft} = -\sqrt{\frac{V_{tot}}{V_{tot}-V_{ads}}} \cdot \frac{2\gamma(T)\cos(\theta)v_l(T)}{RTln(p/p_0)}} \quad (6)$$

And when solving for θ becomes:

$$\boldsymbol{\theta = \arccos\left(\frac{r_{nldft}(RTln(p/p_0))}{-\sqrt{\frac{V_{tot}}{V_{tot}-V_{ads}}}2\gamma(T)v_l(T)}\right)\frac{\pi}{180}}, \quad (7)$$

For water in confinement ~~At~~at 25 ˚C, the values of $\gamma(T)$ and $v_l(T)$ are ~~=~~71.69 mN/m and ~~$v_l(T)$ is~~ 20.5 m^3/mol, respectively (Kocherbitov and Alfredsson, 2007)~~., but differ from the values in bulk water due to being in confinement.~~ When deriving θ, p/p_0 is ~~determined as the relative pressure~~ identified as the saturation ratio ~~-~~where the pore condensation step of the DVS measurement is the steepest~~.-~~

2.3 Ice nucleation measurements

The mesoporous silica particles listed in Table 1 were tested in the Zurich Ice Nucleation Chamber (ZINC), a continuous flow diffusion chamber with a parallel plate geometry. The operating principal of ZINC can be found in Stetzer et al. (2008) and a brief description is given here. Aerosol particles are injected into ZINC where they become sheathed between particle-free nitrogen in a region between two thermally controlled ice-coated walls. By applying a gradient in temperature between the two ice-coated walls, the temperature and supersaturation that the aerosols are exposed to is controlled. Depending on the aerosol properties and the set conditions in ZINC, aerosol particles may nucleate ice and continue to grow as they flow through the chamber until they reach an optical particle counter (OPC; Lighthouse Remote 3104) at the outlet of the chamber that counts and sizes the particles. All particles larger than 1 µm are considered ice crystals and are thus counted as ice nucleating particles at the set conditions in ZINC. To ensure that the particles counted by the OPC are truly ice crystals and not water droplets when conditions exceed water saturation, the particles pass through an isothermal section kept at ice saturation (water

subsaturation) and the temperature equivalent to the warm wall prior to being sampled by the OPC, allowing any formed cloud droplets to evaporate while the ice crystals remain unchanged.

All *RH*-scans between ice saturation and 105 % RH_w were performed with a ramp rate of 2% increase in ice supersaturation per minute. At the start and end point of each scan, a 5-minute background sample was taken by forcing the sample flow through a filter in order to determine the background noise of the chamber. The OPC counts from these background periods were averaged and then linearly interpolated to produce a background that was subtracted from each *RH*-scan (Boose et al., 2016; Burkert-Kohn et al., 2017). An activated fraction (*AF*) is calculated by comparing the number of particles larger than 1 µm exiting ZINC as determined by the OPC ($N_{ice(OPC)}$) and the number of ~~aerosols~~ aerosol particles entering the chamber ($N_{aero(CPC)}$), as counted by a condensation particle counter (CPC, TSI 3787) upstream of ZINC given by:

$$\boldsymbol{AF} = \frac{\boldsymbol{N_{ice(OPC)}}}{\boldsymbol{N_{aero(CPC)}}}. \quad (8)$$

2.4 Aerosol generation

The particles were aerosolized using a rotating brush generator (Palas, RGB-100) supplied with evaporated liquid nitrogen (purity 6.0) to eliminate any residual humidity (*RH* < 1 % at 223 K) and then passed through a 1 µm cyclone (URG-2000-30EHB) to further lower the chance of large particles proceeding through the system before entering a 2.7 m^3 stainless steel tank (Kanji et al., 2013). The tank was filled to a concentration between 4000 and 10000 cm^{-3} and a fan inside the tank ensured that the particles remained suspended. Before entering ZINC the particles were size selected for 400 nm using a custom-built differential mobility analyzer (DMA), which consists of a polonium neutralizer and an electrostatic classifier (TSI 3082 Long Column). Even though the synthesis procedure in this study produces a narrow particle size distribution, the DMA was used to remove any particles larger than 1 µm (from possible aggregation) to reduce the probability of misclassifying dry particles as ice crystals by the OPC.

2.5 Differential scanning calorimetry

In order to determine the ability of a critical ice embryo to fit into the pores of the samples tested, differential scanning calorimetry (DSC; TA Instruments Q10) was performed. The DSC technique detects phase changes based on the heat flow associated with them (e.g., Kumar et al., 2018; Marcolli et al., 2007). Bulk samples were prepared by mixing between 1 and 5 mg of sample with ultrapure water (SigmaAldrich) or deionized water. Deionized water, which has a higher freezing temperature, was used for the large pore samples (9.1H2 and 9.0M2) to achieve a separation between the bulk water and pore water freezing peaks. All DSC experiments were conducted with a cooling rate of 5 K min^{-1}.

3. Results

The results are presented in three sections: the first characterizes the samples tested in this study (Sect. 3.1), the second investigates the ability of particles with 2.8 nm pores to nucleate ice depending on their water contact angle (Sect. 3.2), and the third investigates the role of pore diameter on ice nucleation as a function of surface functionalization (Sect. 3.3).

3.1 Particle characterization

3.1.1 Particle surface area and pore diameter

Nitrogen adsorption and NLDFT provide particle surface area (S_{BET}) and average pore diameter (d_{DFT}), respectively, and are summarized in Table 1 for each sample. The sample naming is such that the initial number represents the average pore diameter in nanometres followed by a C, M, or H to represent whether the sample was calcined, methylated, or hydroxylated, respectively. The numbers 1 or 2 after the letter indicate whether the samples are independent synthesis batches or several batches that have been combined and then separated and functionalized in different ways, respectively. An overview of the pore size distributions of the samples is shown in ~~Fig. 1~~Fig. 2. As evident from ~~Fig. 1~~Fig. 2a., the methylation of the 2.8 nm sample led to a decrease in mean pore diameter by 0.1 nm (2.7M2). The presence of trimethylsilyl groups is confirmed by our DRIFTS measurements (see Sect. 3.1.2), indicating that the methylation was successful. However, we cannot quantify the exact coverage and distribution of the trimethylsilyl groups. The addition of hydroxyl groups to the silica does not produce a difference in the pore size relative to the calcined sample (~~Fig. 1~~Fig. 2a). This suggests that the OH groups do not detectably reduce the pore width or that the pore surface of the calcined sample is already sufficiently hydroxylated, as discussed below.

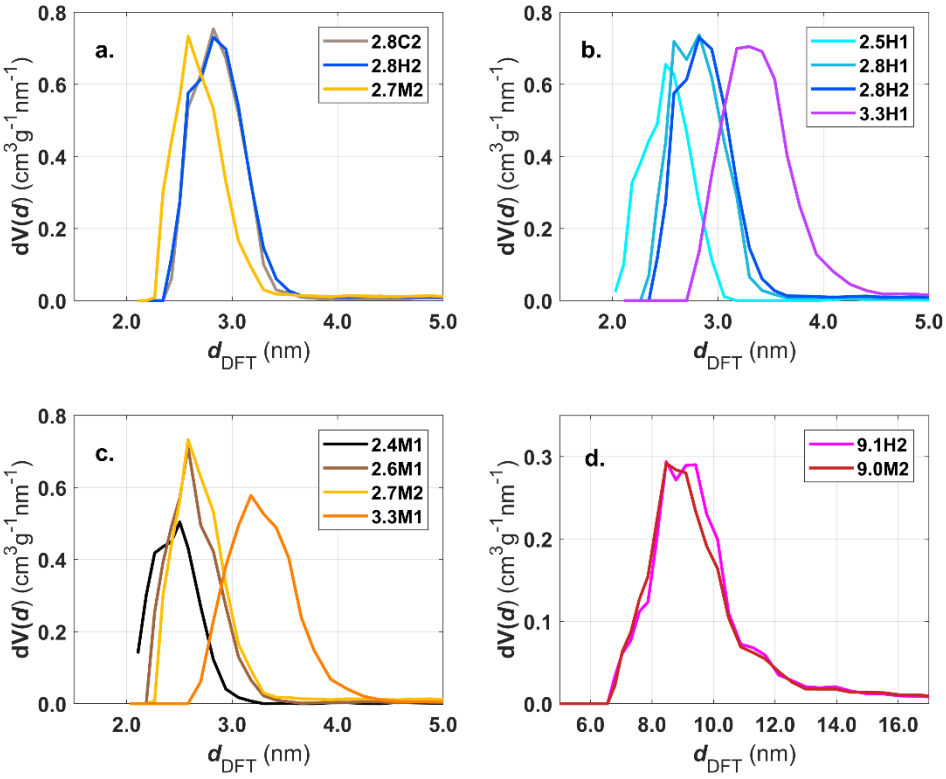

~~Figure 1~~Figure 2: Panel a shows pore size distributions for the 2.8 nm sample after calcination (grey), hydroxylation (blue) and methylation (gold). Panels b and c show pore size distributions of the hydroxylated and methylated samples, respectively. Panel d shows the pore size distribution for the SBA-15 samples after hydroxylation (magenta) and methylation (red).

The pore size distributions of the hydroxylated samples are shown in ~~Fig. 1~~Fig. 2b. The 2.8 nm samples, 2.8H1 and 2.8H2 are quite similar, however 2.8H1 has a larger fraction of 2.6 nm pores. 2.5H1 has the narrowest pore size distribution and the lowest total pore volume of the hydroxylated samples as shown in Table 1. Meanwhile, 3.3H1 has the broadest pore size distribution with pores ranging from 2.7 to 4.5 nm. The methylated samples show a similar trend with a broadening of pore size distribution with increasing average pore diameter (see ~~Fig. 1~~Fig. 2c). Consistent with functionalization, the methylated samples have lower pore volumes than the corresponding hydroxylated samples (see V_{Ptot} in Table 1). This provides additional evidence that the methylation procedure was effective. The SBA samples (9.1H2 and 9.0M2) show a similar trend with a slight decrease in pore diameter upon methylation (~~Fig. 1~~Fig. 2d). As shown in Table 1, there is no relationship between the total BET surface area and pore diameter except when comparing the MCM-41 to the SBA-15 samples which have approximately half of the specific surface area due to their differing morphology and pore structure.

Table 2: Summary of samples used for ice nucleation studies. The BET method was used for total surface area (S_{BET}) and α_s-plot for external surface area (S_{EXT}), (Bhambhani et al., 1972). The total pore volume (V_{Ptot}) was taken at p/p_0=0.95.

Sample Name	Synthesis Method	d_{DFT}	Functionalization	S_{BET} (m^2/g)	S_{EXT} (m^2/g)	V_{Ptot} (cm^3/g)	θ (˚)
3.3M1	MCM-41	3.3 nm (±0.3)	Methyl	726	12	0.50	75-80
3.3H1	MCM-41	3.3 nm (±0.3)	Hydroxyl	893	22	0.66	41-45
2.4M1	MCM-41	2.4 nm (±0.2)	Methyl	822	7	0.33	75-80
2.5H1	MCM-41	2.5 nm (±0.2)	Hydroxyl	892	7	0.38	41-45
2.6M1	MCM-41	2.6 nm (±0.2)	Methyl	917	12	0.42	N/A
2.8H1	MCM-41	2.8 nm (±0.2)	Hydroxyl	1007	15	0.53	N/A
2.7M2	MCM-41	2.7 nm (±0.2)	Methyl	925	13	0.45	N/A
2.8C2	MCM-41	2.8 nm (±0.2)	Calcined	868	12	0.49	N/A
2.8H2	MCM-41	2.8 nm (±0.2)	Hydroxyl	920	14	0.53	N/A
9.0M2	SBA-15	9.0 nm (±1.1)	Methyl	399	N/A	0.95	60-71
9.1H2	SBA-15	9.1 nm (±1.1)	Hydroxyl	429	N/A	0.98	15-37

3.1.2 DRIFTS

When comparing the impact of functionalization on the same initial bulk sample (2.8C2), the difference between hydroxylation (2.8H2) and methylation (2.7M2) is visible in the DRIFTS spectra (~~Fig. 2~~Fig. 3a). The intensity in the O-H stretching region, 3200-3800 cm^{-1}, is much larger for the hydroxylated sample (2.8H2) than the calcined (2.8C2) and methylated (2.7M2) samples, consistent with the addition of hydroxyl groups during the hydroxylation process. The broad absorption band peaking at about 3450 cm^{-1} (3000-3700 cm^{-1}) in the calcined, hydroxylated and methylated samples is indicative of water adsorbed on the silica surface and residual silanol groups (Chen et al., 1996). Previous studies have shown that calcining silica particles at temperatures above 200 ˚C, as is the case for our calcined samples, removes all free water (Muster et al., 2001; Zhuravlev, 2000). However, here the DRIFTS cell was operated at ambient conditions, allowing for water to (re-)adsorb to the particle surface and contributing to the broad absorption in the range 3000 – 3700 cm^{-1} (Muster et al., 2001). Indeed, when exposing a silica sample calcined at 200 °C to ambient conditions, the increase in mass due to adsorbed water is visible using thermogravimetric analysis (not shown). The methylated sample (2.7M2) has the weakest absorbance in the OH stretching region (3000-3700 cm^{-1}; see ~~Fig. 2~~Fig. 3a). Furthermore, the methylated sample shows a peak associated with the C-H stretching band around 2960 cm^{-1}, indicating the presence of trimethylsilyl groups bonded to the silica surface. However, the presence of isolated and geminal silanol groups, as shown by the peak at 3750 cm^{-1}, indicates that the methylation is incomplete (Bergna, 1994; Muster et al., 2001). The increase in the C-H stretching band due to the methylation (at 2960 cm^{-1}), roughly corresponds to the decrease in the isolated silanol/geminal silanol peak for the 2.8 nm samples (~~Fig. 2~~Fig. 3a). The calcined sample (2.8C2) has the highest concentration of isolated and geminal silanol groups. This is expected as during hydroxylation (2.8C2 transitioning to 2.8H2) the concentration of silanol groups increases and becomes sufficiently dense for chains of

hydrogen bonds to form between individual silanol groups, decreasing the number of isolated silanol groups and thereby shifting the peak at 3750 cm^{-1} to ~3660 cm^{-1} (Muster et al., 2001).

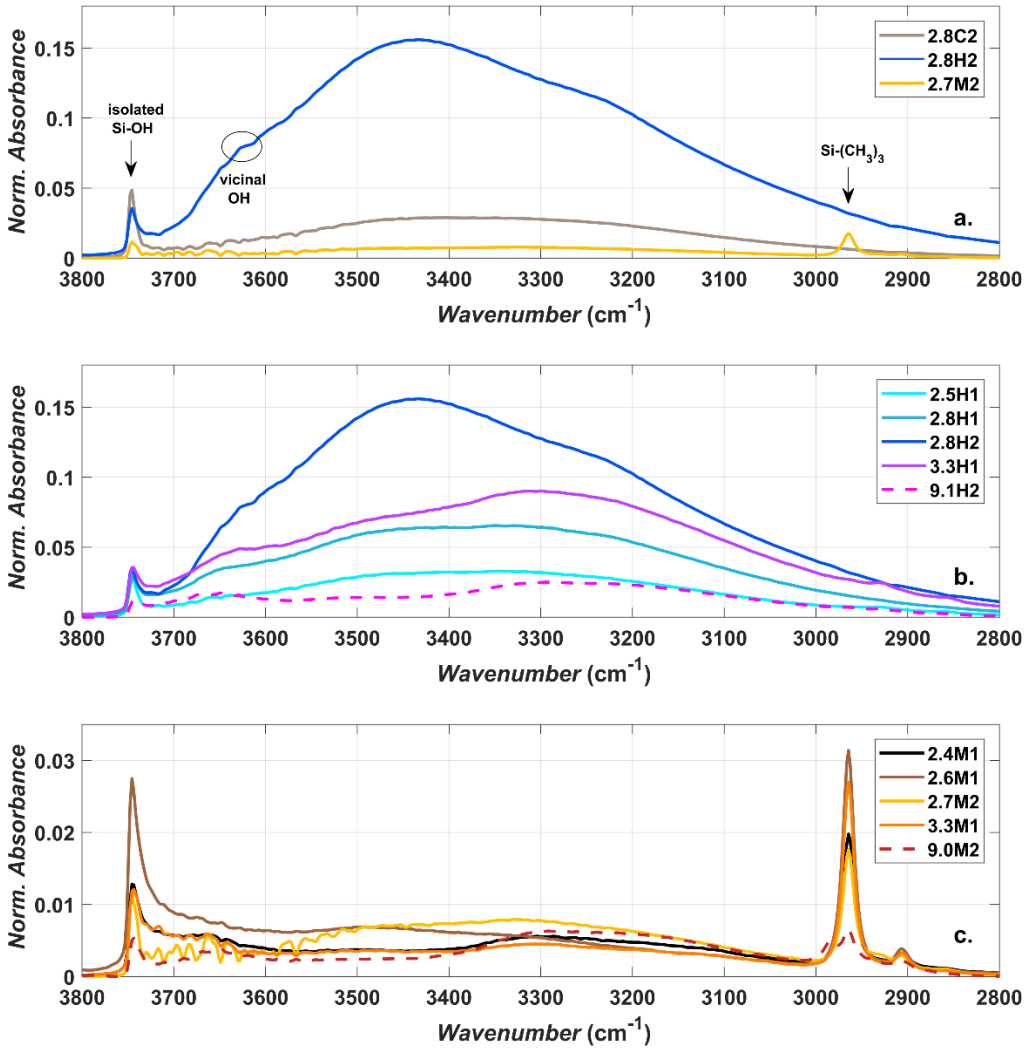

~~Figure 2~~Figure 3: DRIFTS normalized absorbance (Kubelka-Munk) for the 2.8 nm particles after calcination (grey), hydroxylation (blue) and methylation (gold) (panel a). Panels b and c show the spectra of hydroxylated and methylated samples, respectively.

When comparing the DRIFTS results of the different hydroxylated and methylated samples (~~Fig. 2~~Fig. 3b and c), it is clear that the SBA-15 particles (9.1H2 and 9.0M2) also show absorbance in the OH (3200-3800 cm^{-1}) and CH (~2960 cm^{-1}) stretching region of the spectra, respectively, demonstrating that the functionalization was successful. Differing peak intensities between particle types could be due to the differing densities of silanol and siloxanes on the surface of the particles. Although the clear peak in the C-H stretch region of the DRIFTS (~~Fig. 2~~Fig. 3c) shows that the methylation process on the SBA-15 particles (9.1H2 functionalization to 9.0M2) was successful, methylation is far from complete since the peak arising from

isolated/geminal silanol stretching vibrations (3750 cm^{-1}) is still visible in all methylated samples (~~Fig. 2~~Fig. 3c). The concentration of hydroxyl groups on the hydroxylated samples is independent of pore size (~~Fig. 2~~Fig. 3). Rather, the intensity in the O–H stretching region likely depends on the age and exposure of the calcined samples to ambient water vapour. The methylated samples show much less spread in the amount of adsorbed water, suggesting that they are more resistant to hydroxylation and more stable over time (~~Fig. 2~~Fig. 3c).

3.1.3 Water vapour sorption

Two ~~W~~water vapour sorption cycles were ~~isotherms~~ obtained for the samples 2.4M1, 2.5H1, 3.3M1, 3.3H1, 9.1H2 and 9.0M2 and the resultant isotherms are shown in ~~Fig. 3~~Fig. 4. The sorption isotherms have been classified following the recommendation by the International Union of Pure and Applied Chemistry (IUPAC, (Sing, 2009; Thommes et al., 2015). The hydroxylated samples (2.5H1, 3.3H1 and 9.1H2) show Type IV isotherms, characterized by an initial monolayer-multilayer adsorption occurring on the pore wall followed by a steep, almost step-like increase in water mass known as the condensation step at the p/p_0 or *RH* associated with pore filling. This is consistent with previous observations for mesoporous silica (Kittaka et al., 2011). The methylated samples, 2.4M1, 3.3M1 and 9.0M2 show similar isotherms, but lack an initial monolayer adsorption along the uptake curves. This is consistent with a Type V isotherm and provides direct evidence that the methylation was successful in making the particles more hydrophobic. It should be highlighted that in the 2nd sorption cycle, the methylated samples have Type IV isotherms that are more similar to the isotherms of the hydroxylated samples, independent of the pore size. This transition suggests that the exposure to high concentrations of water vapour during the first sorption cycle increases the number of silanol groups on the surface of the methylated samples. Indeed, the second sorption cycle of the methylated samples shows that the condensation step shifts close to the *RH* of the hydroxylated sample during the first sorption cycle. This indicates that the water contact angle of the methylated sample becomes closer to that of the hydroxylated sample. Similarly, the shift in the condensation step to lower humidities for the hydroxylated samples suggests a decrease in water contact angle. The relative mass of the hydroxylated samples does not return to zero after the desorption cycle (~~Fig. 3~~Fig. 4a and b), indicating that water remains adsorbed on the particles. This strongly adsorbed water is expected to lower the water contact angle between water and the wall surface to nearly zero. Moreover, multilayers of adsorbed water narrow the effective diameter for pore filling (Broekhoff and de Boer, 1967; Kruk et al., 1997; Miyahara et al., 2000). Both effects explain the observed shift of the condensation step to lower humidities. Furthermore, it is visible from ~~Fig. 3~~Fig. 4 that the hydroxylated samples adsorb relatively more water than the methylated samples even though they have very similar pore diameters (see d_{DFT} in Table 1). However, the samples have differing total pore volumes (V_{Ptot}) and thus it is expected that the absolute amount of condensed water differs.

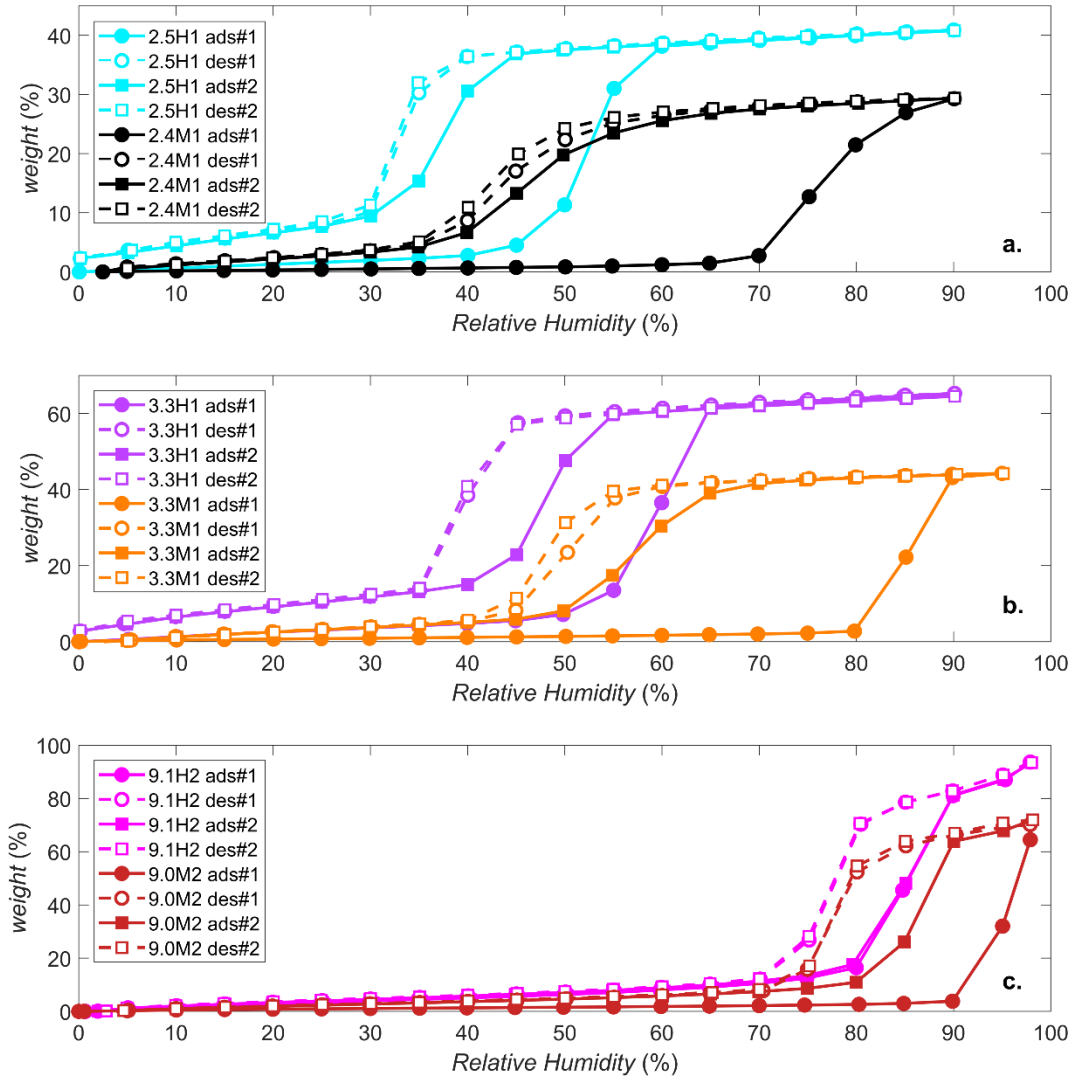

~~Figure 3~~Figure 4: Water sorption isotherms for 2.5H1 (cyan) and 2.4M1 (black) in panel a., 3.3H1 (purple or lilac) and 3.3M1 (orange) in panel b., and 9.1H2 (magenta) and 9.0M2 (dark red) in panel c. The solid and dashed lines with closed and open symbols indicate adsorption and desorption isotherms, respectively. The first and second adsorption/desorption cycles are indicated by circles and squares, respectively.

The water contact angle of the samples is obtained by inserting the *RH* of the condensation step in the first water sorption cycle into Eq. 7 (see Table 1). The water contact angles for the MCM-41 particles ranged between 41˚- 45˚ and 75 ˚- 80˚, for the hydroxylated and methylated samples, respectively, based on the observed value and uncertainty in the measured d_{DFT}. Conversely, the SBA-15 type samples have significantly lower water contact angles of 15˚ and 60˚ for the hydroxylated (9.1H2) and methylated (9.0M2) samples, respectively. However, these values may be due to the large spread ~~of~~ in the pore diameters within the sample. As can be seen from ~~Fig. 1~~Fig. 2, the pore size distribution is significantly wider for the SBA-15 samples than for the MCM-41 particles (ranges from ~7 to 16 nm with a clear ~~mode at~~maximum in the size distribution at 9

nm). Therefore, it is difficult to properly assign the correct pore diameter responsible for the initial pore condensation observed from the sorption measurements based on the uncertainty in d_{DFT} alone (±1.1 nm). If 7 nm is used as the pore diameter instead of 9.1 or 9.0 nm and the *RH* of the initial uptake in pore water from the sorption measurements is used, the water contact angle for 9.1H2 and 9.0M2 become 37˚ and 71˚, respectively.

3.1.4 DSC measurements

Upon cooling of a sample prepared as a slurry in the DSC, the exterior water freezes first followed by the freezing of pore water due to the decrease in temperature required for water in confinement to freeze (Deschamps et al., 2010; Janssen et al., 2004; Jelassi et al., 2010; Kittaka et al., 2011; Marcolli, 2014; Moore et al., 2012; Morishige and Uematsu, 2005). This can most clearly be seen in the freezing of 3.3M1 shown in Fig. ~~4a~~ 5a where the initial release of latent heat (peak) centred around 255 K is due to the freezing of the exterior bulk water followed by the second peak starting at 234 K due to the freezing of the pore water. Tap water was used for the experiments with the SBA-15 samples to shift the freezing of exterior water to higher temperatures so that the freezing of pore water is observable (Fig 4c). Also shown in ~~Fig. 4~~Fig. 5 are the expected critical pore diameters D_p calculated following Eqs. 2 and 3, yielding a direct comparison of the theoretical predictions of pore freezing to the experimentally determined onset of ice formation (peaks in thermograms). Since previous MD simulations and X-ray diffraction studies have shown ice in confinement to be typically stacking disordered or cubic (Moore et al., 2010, 2012; Morishige et al., 2009) two parameterizations from literature (Murray et al., 2010; Zobrist et al., 2007) were used to calculate D_p, assuming either cubic (~~Fig. 4~~Fig. 5a and b) or hexagonal ice (~~Fig. 4~~Fig. 5c). As can be seen in ~~Fig. 4~~Fig. 5, the parameterization assuming cubic ice is more accurate at predicting the observed freezing temperature for narrow mesopores (2.8 and 3.3 nm samples) where the freezing temperatures are around 230 K. ~~Whereas~~ In contrast, the freezing temperature of the 9.1 nm pore samples (9.1H2 and 9.0M2; Fig 4c) of approximately 261 K is better predicted assuming that the ice is hexagonal. These results are consistent with studies that have shown that cubic ice occurs more readily at colder temperatures (Kuhs et al., 2012; L. Malkin et al., 2015).

The DSC thermograms of the SBA-15 samples (9.1H2 and 9.0M2) show a bimodal peak associated with the freezing of pore water (see ~~Fig. 4~~Fig. 5.c), with a pronounced peak around 258 K and a shoulder towards higher *T*. This indicates that there is a bimodal distribution of pore sizes that contribute differing fractions of pore volume to the samples. Indeed, the pore size distributions show that the SBA-15 samples have a clear shoulder in the distribution at 11 nm followed by a main peak at 9.1 nm (see ~~Fig. 1~~Fig. 2.d). Thus the bimodal freezing signal is likely due to the freezing of pore water in pores larger than 11.0 nm followed by the release of heat from the freezing in the smaller, more abundant 9.1 nm, remaining pores.

Deschamps et al., (2010) showed that highly hydrophobic pore surfaces had lower melting and freezing temperatures than hydrophilic pores of the same diameter. They associated the depressed freezing temperatures with a decrease in mobility of

water molecules in hydrophobic mesopores. However, as the pore size exceeded 3 nm, the dependence on pore-hydrophobicity of the freezing point depression disappeared (Deschamps et al., 2010; Jähnert et al., 2008; Schreiber et al., 2001). In agreement with a loss of the dependence on hydrophobicity for pores larger than 3 nm, Moore et al, (2012) showed that the melting temperature in a 4 nm diameter silica pore was the same regardless of hydrophobicity using MD simulations. The DSC thermographs in ~~Fig. 4~~Fig. 5 show that there is no detectable difference in the onset freezing temperatures for the SBA-15 samples depending on functionalization (9.1H2 and 9.0M2; ~~Fig. 4~~Fig. 5c). However, in contrast to the results of Deschamps et al. (2010), the 2.8 nm (~~Fig. 4~~Fig. 5b) samples also show no detectable difference in freezing onset. This indifference may stem from the fact that the observed freezing onsets occur due to the ice growth in the largest detectable pores of a sample. As can be seen from ~~Fig. 1~~Fig. 2, both 2.8H2 and 2.7M2 contain a fraction of pores larger than 3 nm. Therefore, the observed freezing onsets in the thermograms may be due to pore diameters that are wide enough for growing ice to not be impacted by the water contact angle of the pore wall (Moore et al., 2012).

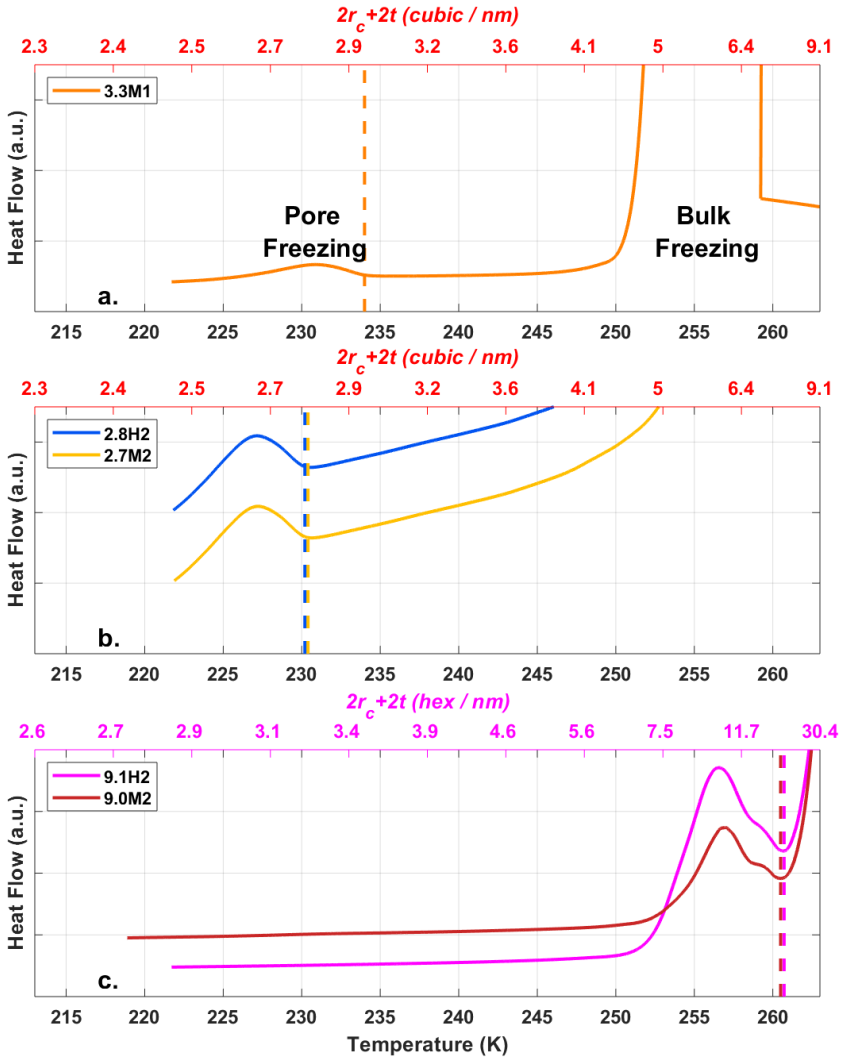

~~Figure 4~~Figure 5: **DSC thermograms for ice growth into pores for samples 3.3M1 (panel a), 2.8H2 and 2.7M2 (panel b), and 9.1H2 and 9.0M2 (panel c). The vertical dashed lines mark the observed onset temperatures of pore freezing. The upper x-axes represent the predicted critical pore diameter *($2r_c+2t$)* for cubic (red axis labels, panel a and b) or hexagonal (magenta axis labels, panel c) ice to be stable, following Marcolli (2014). The peak on the right-hand side of panel a and the descending lines in panel c are due to the bulk freezing of exterior water.**

3.2 Pore condensation and freezing experiments: the 2.8 nm pore example

A summary of the ice formation activity of the functionalized 2.8 nm particles from a single batch (2.8H2, 2.8C2 and 2.7M2) is shown in ~~Fig. 5~~Fig. 6, where the RH_i required for an *AF* of 0.05 ($AF_{0.05}$) are shown. An *AF* of 0.05 was chosen as best

representing the average freezing *RH* of the porous particles. The complete *AF* curves are shown in Appendix A1. The onset RH_i at 223 and 228 K is significantly lower for the hydroxylated (blue) and calcined (grey) samples than for the methylated sample (gold). This reveals a strong dependence on the water contact angle, which is lower in case of the hydroxylated sample (θ = 41˚ - 45˚) compared to the methylated sample (θ = 75˚ - 80˚). The lower onset humidity of the hydroxylated sample is consistent with the inverse Kelvin effect, which predicts pore filling to occur at a lower RH_i for the hydroxylated sample. Furthermore, the pore filling line based on Eq.1 for the methylated sample (assuming θ = 78˚), predicts the observed freezing onsets at 223 and 228 K (gold line, $AF_{0.05}$), respectively, within experimental uncertainty, indicating that the PCF mechanism is limited by pore filling. Additionally, this suggests that the ice formed in the methylated pores investigated here is capable of growing into the unconfined vapour region as proposed by David et al. (2019) without the need for a two-step nucleation process (Christenson, 2013; Kovács and Christenson, 2012; Page and Sear, 2006). In contrast, the 2.8 nm hydroxylated sample (2.8H2) is predicted to fill below ice saturation ($RH_i \geq$ 71 % at 223 K and $RH_i \geq$ 69 % at 228 K). Therefore, ice growth should be observed as soon as ice saturation is exceeded within ZINC, yet a RH_i of 118% (223 K) and 112 % (228 K) is required to observe an $AF_{0.05}$ (~~Fig. 5~~Fig. 6). This might suggest that a two-step nucleation mechanism is required for ice to grow out of narrow calcined and hydroxylated mesopores at these lower supersaturations (Campbell et al., 2017; Christenson, 2013). However, particles must grow to at least 1 µm before they are detected as ice crystals in this study (see Section 2.3). Hence, the limited growth time in ZINC (~10 seconds) for the particles to reach a size of 1 µm must be accounted for when interpreting ice onset. Therefore, we calculated theoretical ice growth curves (dashed salmon~~peach~~ lines, see A2 for calculation) using the parameterization from Rogers and Yau (1989) and assuming accommodation coefficients of 0.1 and 0.2 for ice growth at $T <$ HFT (Earle et al., 2010; Isono and Iwai, 1969; Magee et al., 2006; Skrotzki et al., 2013). The ice crystal shape in the growth calculation was assumed to be spherical due to the small final size (~1 µm) and its growth on spherical particles (Harrington et al., 2019). Comparing our ice onsets to the expected growth (dashed salmon~~peach~~ lines, ~~Fig. 5~~Fig. 6), the slow ice crystal growth may explain~~s~~ the required RH_i to observe ice within the ZINC experiments, without the need of a two-step nucleation mechanism (David et al., 2019). Moreover, the reported *AF* of 0.05 do not correspond with the ice onset. Considering Fig. A1, the initial ice observed is at RH_i 110 % and 108% for 223 and 228 K, respectively. Lupi et al., (2017) and Moore et al., (2010) have shown in MD studies that stacking disordered ice is formed in confinement and during nucleation, requiring a humidity higher than 100% to grow ice. Additionally, the calculated humidity that particles are exposed to in ZINC depends on the temperatures of the warm and cold walls, which are measured by thermocouples that have an uncertainty of ±0.1 K (Stetzer et al., 2008). This uncertainty (±5 %) can lead to a higher reported humidity than required to observe ice nucleation and is included in the vertical error bars in Figure 6, 7 and 8.

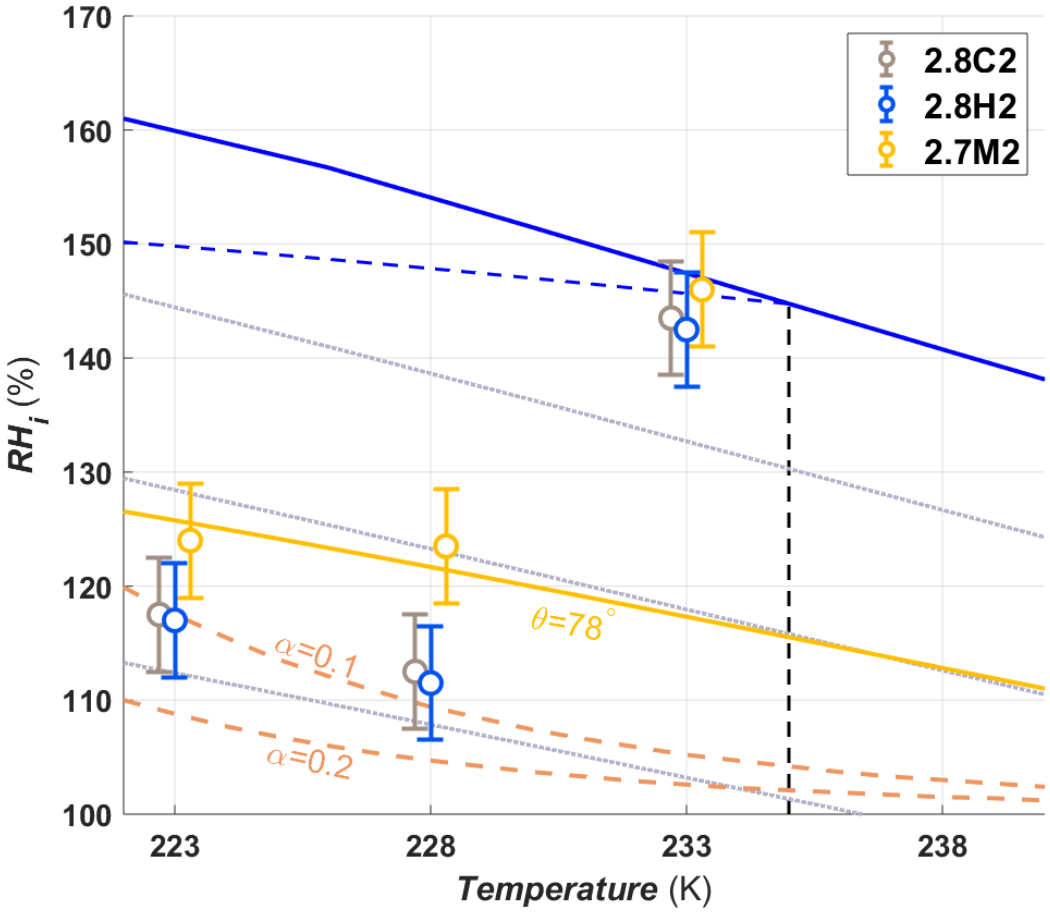

~~Figure 5~~Figure 6: **The average RH_i required for an $AF_{0.05}$ for the hydroxylated (blue), methylated (gold) and calcined (grey) porous (2.7 – 2.8 nm) silica samples. The error bars represent the maximum uncertainty in the calculated RH_i (±5 %)~~uncertainty~~ in ZINC arising from the uncertainty in the reported thermocouple temperature (±0.1 K; Stetzer et al., 2008) and encompass the standard deviation from averaging the experiments. The solid blue line and dotted grey lines represent water saturation and constant RH_w decreasing in steps of 10 % from the water saturation line respectively. The dashed blue line is the homogeneous nucleation RH_i based on Koop et al. (2000) assuming a nucleation rate of 10^8 cm^{-3} s^{-1}. The vertical dashed black line represents the homogeneous freezing temperature of pure water (HFT). The golden line denotes pore filling of 2.7 nm wide pores assuming a water contact angle of $\theta = 78^\circ$. Pores of the hydroxylated and calcined samples are expected to fill well below ice saturation. The dashed salmon lines indicate the required RH_i for ice to grow to a detectable size within the residence time of ZINC assuming an accommodation coefficient (α) of 0.1 or 0.2, respectively. Measurements were also conducted at 238 K but an $AF_{0.05}$ was not detected. The symbols of the calcined and methylated samples are offset by 0.3 K colder and warmer, respectively, for clarity.**

In a PCF mechanism it is expected that once the critical humidity for pore filling is reached, ice nucleation and growth should lead to a step-like increase of *AF* to values close to unity. Yet the increase in RH_i between onset and $AF_{0.05}$ (Figs. A1 and A2) indicates that either the pores on the particles are not homogeneous in both pore size and/or water contact angle or the conditions within ZINC are non-uniform. Indeed, Garimella et al. (2017) showed that turbulence at the entrance of the chamber causes particles to leave the (predicted) aerosol lamina and therefore, these particles experience a lower RH_i than the ones in

the lamina. The assumption that all particles are within the lamina leads therefore to a low bias of *AF* at all RH_i and a shift of *AF*=1 to higher RH_i. The underestimation of *AF* depends on the set temperature and ice supersaturation (gradient between the wall temperatures). At 233 K and 102% RH_w only 78% of the particles were shown to be exposed to the set conditions in ZINC (Garimella et al., 2017). Particles deviating from the lamina likely explain the gradual increase of *AF* with increasing RH_i.

The shift of $AF_{0.05}$ close to water saturation at 233 K (~~Fig. 5~~Fig. 6) is consistent with the DSC measurements which show that the pore water only starts to freeze at 230 K for 2.7 – 2.8 nm pore diameter samples (~~Fig. 4~~Fig. 5b), suggesting that the pores are too narrow for PCF to occur at 233 K. Rather bulk water on the particle surface is required for homogeneous freezing consistent with the observed shift of $AF_{0.05}$ to water saturation at 233 K.

When examining the entire *AF* curves at 233 K shown in Figs. A1c and A2c, there is a clear increase in *AF* to approximately 0.02 for the hydroxylated sample (2.8H2) between 100 and 120% RH_i, and a slight increase of 0.002 for the methylated sample (2.7M2). This suggests that a fraction of the pores small enough to remain undetected in the DSC (see Section 3.1.4) nucleate ice homogeneously at 233 K because they exhibit diameters > 3 nm which is large enough to accommodate the critical ice germs. Such an assumption is in agreement with the tail of pores with d_{DFT} > 3 nm appearing in the pore size distribution of the samples in ~~Fig. 1~~Fig. 2.a. Following Marcolli (2014) for calculating D_p (see Eq. 3), cubic or stacking disordered ice should be stable in pores of approximately 3 nm diameter at 233 K (see ~~Fig. 4~~Fig. 5.b; Moore et al., 2010; Morishige et al., 2009). However, even if the pore diameter is large enough to host a critical ice germ, ice may fail to form during the residence time in ZINC when the nucleation rate within the pore water is too low. Using rates for homogenous ice nucleation derived from experiments ($J_{hom}(T)$; Atkinson et al., 2016; Ickes et al., 2015; Riechers et al., 2013), the residence time in ZINC (t_{ZINC}) for a given pore volume (V_{pore}) to nucleate ice can be calculated as:

$$t_{ZINC} = \frac{-\ln(1-AF)}{J_{hom}(T)V_{pore}}. \quad (9)$$

Using $J_{hom}(T)$ of $10^{10\text{-}12}$ $cm^{-3}s^{-1}$ at 233 K as reported in literature (Ickes et al., 2015; Koop and Murray, 2016; Murray et al., 2010), and V_{pore} based on a single pore with average width and the length of an average particle (400 nm), the residence time in ZINC would need to be 3 to 4 orders of magnitude longer than the ~ 10 s available in order to reach $AF_{0.05}$. Therefore, the observed increase in *AF* to 0.02 for 2.8H2 (Fig. A1c) does not comply with reported homogeneous ice nucleation rates, but may be explained by the effect of pressure. As *RH* decreases, tension (negative pressure) builds up in the pore water as a function of the curvature of the water meniscus at the pore opening, such that nucleation rates increase drastically (Marcolli, 2020). At the *RH* of pore filling (RH_w = 67 %), the pore water experiences a strongly negative pressure (-83 MPa). At 233 K and water saturation (*P* = 0.1 MPa), the pressure-dependent extension of the Murray et al. (2010) parameterization of CNT (Marcolli, 2020) predicts a nucleation rate of $9 \cdot 10^{10}$ $cm^{-3}s^{-1}$ (when using an exponent of n = 0.97 for estimating σ_{iw} following Murray et al., (2010)). However at RH_w = 67 % (*P* = -83 MPa) the nucleation rate increases to over 10^{21} $cm^{-3}s^{-1}$ ($4 \cdot 10^{22}$ $cm^{-3}s^{-1}$), which should result in freezing of pore water in less than a millisecond. Note that the dry particles that are injected into ZINC reach ice saturation condition within the chamber after about 0.5 s and water saturation condition after about 1 s (Stetzer et al.,

2008). Thus, there should be enough time for pore water to freeze before equilibrium conditions are reached for those pores that are wide enough to host ice.

At 238 K, the 2.8 nm samples discussed in this section (2.8H2, 2.8C2 and 2.7M2) do not reach $AF_{0.05}$ even above water saturation (Fig. A1.d and A2.d). Only as the RH_i approaches and exceeds water saturation the *AF*s of 2.8H2 and 2.7M2 reach 0.04 and 0.006, respectively (Figs A1d and A2d). The curves of the hydroxylated samples show a weak increase that steepens when water saturation is approached (Fig. A1d), which we ascribe to condensation or immersion freezing (Vali et al., 2015) occurring at active sites on the external particle surface. Pore water is likely not responsible for the observed freezing when the entire particle is immersed in water (Campbell et al., 2015). Furthermore, as temperature increases, the critical ice germ size increases and therefore, a larger pore diameter is required for PCF to occur at 238 K than at 233 K independent of the presence of active sites in the pore. Based on the DSC thermograms shown in ~~Fig. 4~~Fig. 5a, even the samples with pore diameters of 3.3 nm have freezing onsets below 238 K. Moreover, 9.1H2 with pore diameters large enough to accommodate the critical ice embryo based on the DSC measurements (see ~~Fig. 4~~Fig. 5c) is least efficient at freezing (see Fig. A1d). Therefore, the observed freezing is likely due to nucleation sites on the outer particle surface that become active when immersed in water. This assumption is further substantiated by experiments performed with nonporous silica particles which showed similar ice nucleation activity as their porous counterparts (not shown) at 238 K. The ability of these active sites to nucleate ice is reduced on the methylated sample (see Fig. A2), consistent with previous studies that suggest that hydroxyl groups are important for templating ice formation (Pedevilla et al., 2017) and alkylated silica surfaces suppress ice nucleation (Kanji et al., 2008).

3.3 Role of pore diameter on PCF

In order to investigate the ability of the pore diameter to influence the PCF mechanism, particles with different pore diameters were synthesized with either hydroxyl or trimethylsilyl surface groups and we discuss these separately in the following.

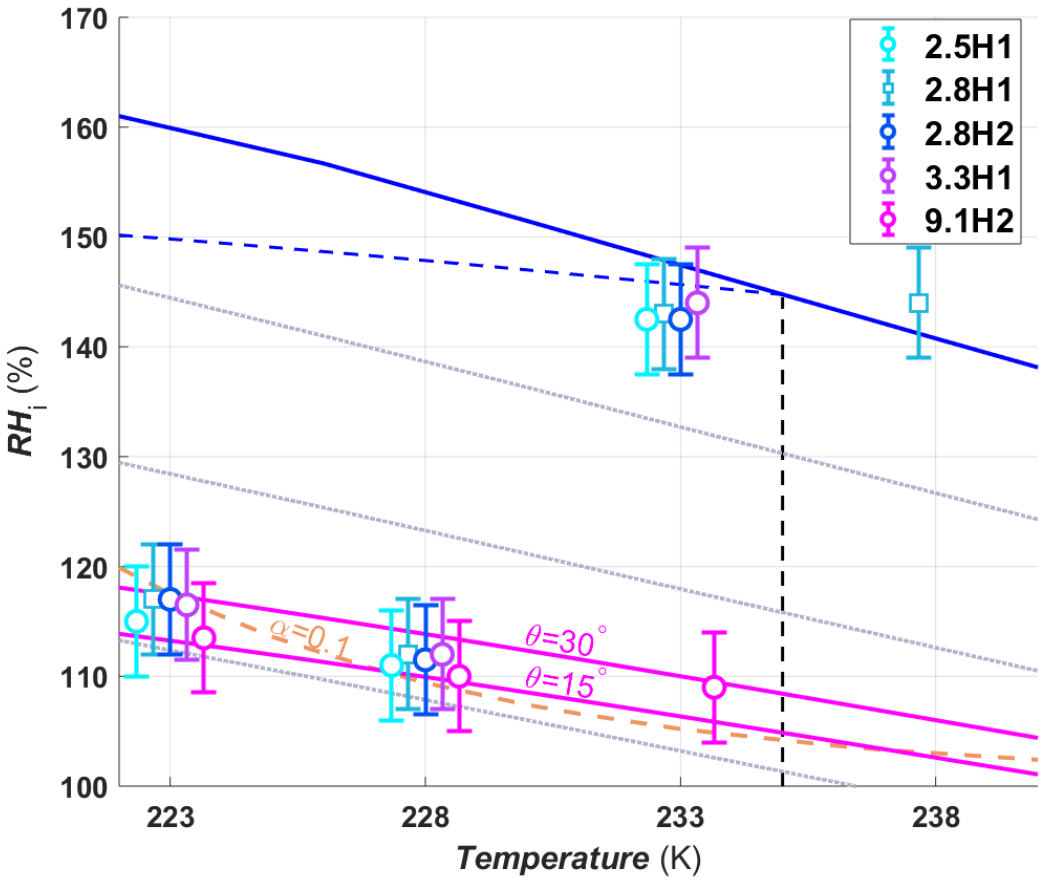

~~Figure 6~~Figure 7: **Average RH_i required to reach an $AF_{0.05}$ ~~conditions~~ for hydroxylated silica samples of different pore diameters. The symbols are offset by ± 0.3 or 0.6 K from the experimental temperatures to make the points more visible. The pore filling lines are plotted for 9.1 nm pores assuming a water contact angle of 15 and 30˚ (magenta lines). Symbols and reference lines are as in ~~Fig. 5~~Fig. 6.**

3.3.1 Hydroxylated samples

Pore diameter has no impact on the humidity required for the hydroxylated samples to reach $AF_{0.05}$ below the HFT (~~Fig. 6~~Fig. 7, dashed back line), the only exception being at 233 K, where ice formation starts well below water saturation for the 9.1H2 sample, while the smaller pore size samples reach $AF_{0.05}$ only close to water saturation. This is indeed expected for pores up to 3.3 nm, when considering that the water contact angle of the pore surface is rather low for the hydroxylated samples (41 - 45˚; see Sect. 3.1.3), such that the pores are expected to fill already below ice saturation. Assuming that 9.1H2 has a similar water contact angle as the other hydroxylated samples, the 9.1 nm pores would require a RH_i of ~123 and 118 % at 223 and 228 K, respectively, for pore filling to occur. However, based on the water sorption measurements (see ~~Fig. 3~~Fig. 4c) the estimated water contact angle of 9.1H2 is approximately 15˚. Furthermore, when examining the pore size distribution shown

in ~~Fig. 1~~Fig. 2d, more than 5 % of the pores are smaller than 9.1 nm (between 7 and 9 nm) and thus a lower humidity for pore filling is required for these pores. Based on the lower water contact angle alone, the 9.1 nm pores are expected to fill at ~114 and 109 % RH_i at 223 and 228 K, respectively. Therefore, no significant dependence of $AF_{0.05}$ is expected for the investigated samples at 223 and 228 K due to the ice growth limitations in ZINC, as discussed above.

At 233 K the $AF_{0.05}$ RH_i shifts to water saturation for all samples except for 9.1H2 (~~Fig. 6~~Fig. 7). The DSC experiments with 3.3M1 show that ice freezes within the pores only below 233 K (~~Fig. 4~~Fig. 5a). Therefore the inability for 5% of the particles to freeze up to water saturation for these samples, is consistent with PCF.

In contrast, the pore diameters in the 9.1H2 sample are wide enough to host ice at 233 K (see DSC experiments, ~~Fig. 4~~Fig. 5c). Yet, nucleation rates at this temperature are too low for pore water to freeze within the residence time of ZINC. However, the strong increase of *AF* at about 108 % RH_i together with the decrease starting from 125 % RH_i (see Fig. A1c) can be explained by the dependence of nucleation rates on pressure (Marcolli, ~~2019~~2020). At 233 K, the pressure dependent version of the Murray et al., (2010) parameterization of CNT (Marcolli, 2020) predicts a nucleation rate of $9 \cdot 10^{10}$ $cm^{-3}s^{-1}$ at water saturation (P = 0.1 MPa), which increases to $2 \cdot 10^{16}$ $cm^{-3}s^{-1}$ at RH_i of pore filling (~108 % RH_i , P = -32 MPa). Thus, the water in a pore of 9.1 nm diameter should freeze at 108 % RH_i within about 1.6 s. At water saturation, it takes one pore $4 \cdot 10^5$ s to freeze, implying that most pores should freeze at 108 % RH_i within the residence time of ZINC and that *AF* decreases when water saturation is approached as can be seen in Fig. A1c.

At 238 K only the 2.8H1 sample reached an $AF_{0.05}$ (~~Fig. 6~~Fig. 7). However, all of the other hydroxylated samples with the exception of 9.1H2, have a similar increase in *AF* near water saturation reaching values just below the $AF_{0.05}$ threshold (Fig. A1d). This indicates that there are active sites located on the external particle surface that nucleate ice through immersion or condensation freezing rather than PCF. Considering that pores are closely spaced, the outer surface is cladded in pore openings, providing a nanoscale pattern that might influence the ice nucleation activity in immersion and condensation mode.

The SBA-15 sample 9.1H2 also showed an increase in *AF* near water saturation, albeit the increase was about an order of magnitude lower than for the MCM-41 samples (Fig. A1d). Thus, the 9.1H2 surface seems to be less efficient at nucleating ice than the one of the MCM-41 samples, indicating that the synthesis procedure for SBA-15 particles (see Sections 2.1.1 and 2.1.2), generates less active sites than the one for MCM-41 samples. This is especially true when considering that the pores in the MCM-41 samples are too narrow to host the critical ice embryo and therefore, the surface area is significantly smaller than for the 9.1H2 sample. In experiments performed at 243 K the ability of the hydroxylated samples to nucleate ice approached the detection limit of ZINC and are therefore not shown.

3.3.2 Methylated samples

Unlike the hydroxylated samples, the methylated samples show a dependence of onset humidity on pore diameter. At 223 and 228 K, the samples with 2.4 nm pore diameters had the lowest $AF_{0.05}$ RH_i and the 3.3 nm particles the highest. The ~~followed~~

~~by the~~ 2.6, 2.7~~,~~ and 9.0 nm samples~~, which~~ are in-between and overlap ~~, and lastly the 3.3 nm sample~~ (~~Fig. 7~~Fig. 8). This indicates that due to the higher water contact angles after methylation (60˚ – 71˚ compared with 15˚ – 37˚ for the hydroxylated samples), PCF is limited by pore filling ~~rather than ice growth due to the detection limit of ZINC~~the OPC. Thus, the increase in RH_i required for filling of increasing pore diameters, is observable within ZINC for methylated samples. The similar $AF_{0.05}$ RH_i of 9.0M2 at 223 and 228 K compared with the methylated MCM-41 samples can be explained by its lower water contact angle (60˚ vs. 78˚, see Table 1) suggesting a more hydrophilic surface of 9.0M2 compared with MCM-41. The 9.0M2 is less active than the 9.1H2 sample (see Figs. 6 and 7), indicating that the methylation and ~~subsequent~~ associated increase in water contact angle decreased the ice nucleation ability.

Unlike the hydroxylated samples at 233 K, which showed a clear increase in *AF* at ~ 105 % RH_i (Fig. A1c), the methylated samples (except 9.0M2) show only a weak and continuous increase in *AF* up to approximately 0.01 before water saturation is reached and homogeneous freezing of bulk water sets in (see Fig. A2c). This difference is likely due to the higher humidity required for pore filling of the methylated samples. The pore water experiences just a moderately negative pressure of at most -26 MPa at pore filling conditions, which enhances nucleation rates to a level that is able to induce freezing in only very few pores that also need to be wide enough to host ice. The reduction in *AF* below water saturation of the methylated compared with the hydroxylated samples is consistent with previous observations that alkylation of silanol groups suppressed ice nucleation below water saturation at 233 K (Kanji et al., 2008).

The $AF_{0.05}$ of 9.0M2 is close to the predicted pore filling line for $\theta = 78^\circ$ at 233 K (~~Fig. 7~~Fig. 8), while at 223 and 228 K, it is much below the predicted line even for $\theta = 60^\circ$. This freezing activity is attributed to either non-uniform methylation which led to variations in water contact angle or the presence of pore-like imperfections on the rough surface of the 9.0M2 particles that are narrower than the measured pore diameters and remained undetected in the pore-size distribution (~~Fig. 1~~Fig. 2) due to their extremely small volumes. At 233 K, the onset humidity of the 2.7M2 shifts close to water saturation in accordance with the DSC results in ~~Fig. 4~~Fig. 5 showing that ice only freezes close to or below 233 K for pores narrower than 3.3 nm (see Fig. A2). A clear onset RH_i where the bulk of the 9.0M2 particles nucleate ice is absent (Fig. A2c) as is observed with 9.1H2 in Fig. A1c, indicating that pores of 9.0M2 continuously fill and freeze while RH increases. Indeed, the measured pore diameters by N_2 sorption (see ~~Fig. 1~~Fig. 2d) show a wide pore size distribution for 9.0M2 and 9.1H2. Water uptake reaching 1 wt% only above 90 % RH_w for 9.0M2 (~~Fig. 3~~Fig. 4), is in accordance with *AF* exceeding 0.05 only for RH_i > 130 % further supporting that ice nucleation on 9.0M2 is limited by pore filling. Since homogeneous nucleation rates close to water saturation at 233 K are rather too low to induce freezing of water in 9.0M2 pores, ice nucleation sites for immersion freezing within the pores might be responsible for the observed *AF*. The assumption of nucleation sites on the 9.0M2 is further supported by its ice nucleation activity persisting above the HFT (Fig. A2d).

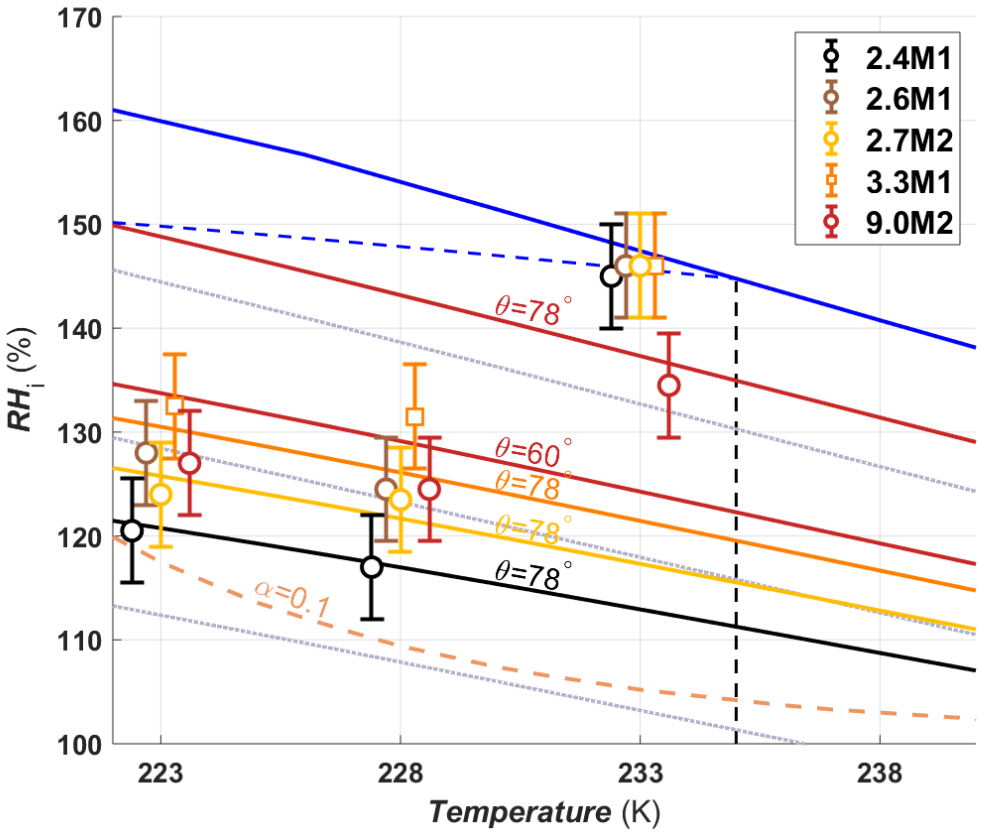

~~Figure 7~~Figure 8: Average RH_i required to reach an $AF_{0.05}$ ~~: Ice formation onset conditions~~ for methylated silica samples of different pore diameters. The symbols are offset by ± 0.3 or 0.6 K from the experimental temperatures to make the points more visible. Pore filling lines are given for 2.4 (black line), 2.7 (gold line), and 3.3 (orange line) nm pores assuming a water contact angle of 78°. For 9.0 nm pores the pore filling lines are plotted assuming water contact angles of 60° and 78° (red lines).

The methylated MCM-41 samples have a very weak increase in *AF* around water saturation at 238 K (Fig. A2d), reaching similar *AF* as at 233 K below water saturation. The increase of *AF* for MCM-41 samples at 238 K is lower than the one observed for the hydroxylated MCM-41 samples at the same temperatures and relative humidities, consistent with the notion that methylation decreases the ice nucleation activity of a surface (Kanji et al., 2008).

At 238 K, the 9.0M2 sample shows a distinct and continuous increase of *AF* below water saturation. Since the temperature is too high for homogeneous ice nucleation within pores, this is a clear indication of active sites present in pores resulting in immersion freezing as soon as the pores fill with water. Interestingly, the *AF* is higher in 9.0M2 compared with 9.1H2 (Fig. A2d and Fig. A1d, respectively), showing that the density of hydroxyl groups is not always a good predictor for ice nucleation ability. Indeed, it has been shown that methylated amorphous silica has an enhanced nucleation ability relative to hydroxylated silica due to the condensation of water on a hydrophilic Si-OH group surrounded by methylated groups (Bassett et al., 1970; Salazar and Sepúlveda, 1983). Salazar and Sepúlveda, (1983) postulated that adsorption on islands of silanol groups followed

by multilayer growth similar to condensation of water would nucleate ice when water molecules come in contact with the neighbouring methyl groups. However, it is important to note that hydroxylation and methylation had an opposite effect on the heterogeneous ice nucleation ability at 238 K of MCM-41 and SBA-15 particles, making generalization in terms of dependence on water contact angle and degree of hydroxylation difficult. The MCM-41 samples are spherical (Fig 1~~8~~a and b) and the pore entrances are evenly distributed over the entire particle surface. Meanwhile, the SBA-15 samples are hexagonal and consist of a 2-D network of pores oriented along the long-axis of their geometry (Fig. 1~~8~~c and d) and thus, potentially have six pore free faces where the interaction between silanol islands and surrounding trimethylsilyl groups is possible. Thus, the potential presence of nonporous faces on the SBA-15 samples could explain the difference in the role of methylation and hydroxylation on the heterogeneous freezing abilities of the sample types at 238 K.

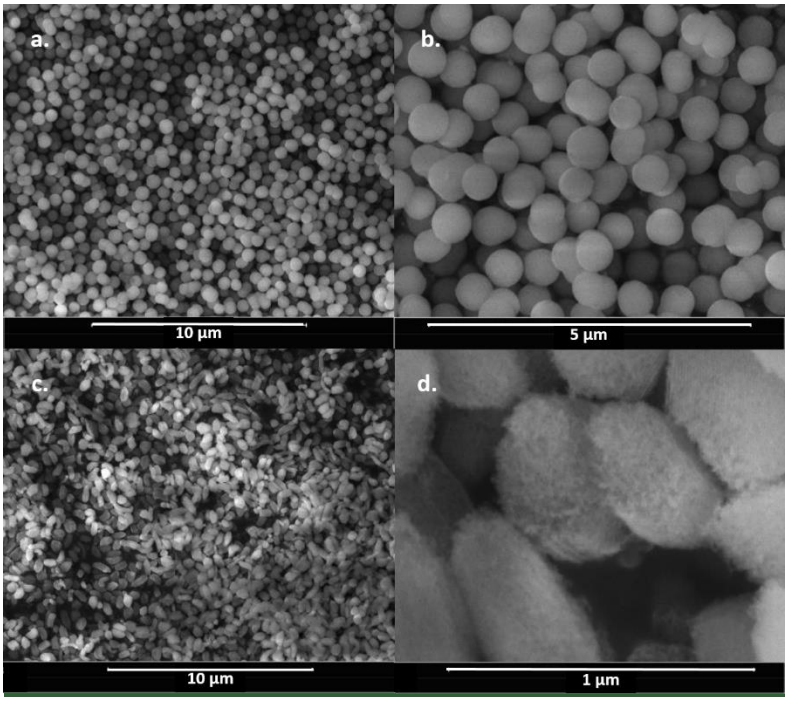

~~**Figure 8**: Scanning electron microscopy images of 2.8H2 (a. and b.) as an example of MCM-41 particles and 9.0M2 (c. and d.) as an example of SBA-15 particles.~~

4. Summary and conclusion

In this study we have investigated the mechanism of pore condensation and freezing and its dependence on pore diameter and water contact angle using synthesized silica particles with well-defined pore diameters. Particle wettability/water contact angle was systematically varied through functionalizing the silica particles with hydroxyl and trimethylsilyl surface groups. The functionalized particles were characterized by N_2 and water vapour sorption, DRIFTS and DSC measurements. Ice nucleation experiments on the porous particles were performed in a continuous flow diffusion chamber, covering a *T* range of 223-238 K

and a relative humidity range of 100 % RH_i to 105 % RH_w, and observed ice nucleation was compared to that predicted by PCF.

The experiments show that the presence of pores together with their diameters and water contact angle are good predictors for the ice nucleation ability of particles below the HFT and below water saturation. The PCF mechanism framework accurately predicts ice nucleation at these conditions. Furthermore, the observed ice nucleation below the HFT did not support a so-called two step nucleation process confirming our previous observations using similar particle types (David et al., 2019).

Above the HFT, ice nucleation within pores cannot occur homogeneously, instead rare active sites can promote heterogeneous nucleation resulting in a lower probability of ice nucleation compared to PCF at T < HFT. Therefore, above the HFT, porosity is no longer a predictor for ice nucleation and the observed ice nucleation activity needs to be explained by the surface functionalization i.e. hydroxylation or methylation and the associated presence of so-called active sites. The enhancement in freezing due to the presence of hydroxyl or methyl groups depended on the sample type, with hydroxylated surfaces enhancing ice nucleation on the MCM-41 particles (spherical particles with pore diameters 2.4 – 3.3 nm) and methylation enhancing ice nucleation in the presence of SBA-15 particles (non-spherical of ~ 9nm pore diameter). Although the two particle types are composed of the same material, silica, the differing effect of the functional groups indicates that the role of functional groups depends on the specific surface structure. Ice nucleation at 238 K mainly occurred at water saturation, indicating that immersion or condensation freezing was the responsible mechanism.

In summary, the ability of particles to nucleate ice below water saturation at cirrus conditions can be predicted by the particle pore size distribution and water contact angle. Therefore, ice nucleation parameterizations should include the PCF mechanism below the HFT. Above the HFT, active sites present on the particle surface determine the ice nucleation activity at water saturation, while below water saturation active sites within pores are required to nucleate ice.~~Therefore, ice nucleation parameterizations should be based on PCF below the HFT while above the HFT the presence of active sites determines the ice nucleation activity at water saturation, while the availability of active sites within pores may give rise to ice nucleation below water saturation~~. In the troposphere, mineral dust particles which are generally hydrophilic with low water contact angles will nucleate ice via PCF and the extent of which will depend on factors such as pore size distribution and shape, water contact angle and any coatings on the dust particles. Therefore, we recommend that future studies should focus on characterizing particle porosity and water contact angle to better assess the role of pores on ice nucleation. We also recommend that future studies investigate the role of atmospheric aging and coatings on PCF. Certain coatings can lower the freezing point of pore water or completely block pores, inhibiting particles from nucleating ice. Thus, understanding the role of atmospheric aging on the ability of porous particles to nucleate ice via PCF is essential for understanding how anthropogenic emissions, such as soot, which has been shown to nucleate ice in accordance with PCF (Mahrt et al., 2018, 2020b, 2020a; Nichman et al., 2019), will impact future climate.

Author Contributions: R.O.D wrote the manuscript with contributions from C.M, Z.A.K, J.F and F.M. R.O.D conducted the ice nucleation measurements with help from F.M. R.O.D analysed the ice nucleation data. J.F and D.B synthesized and characterised the particles with varying pore diameters and functional groups. R.O.D interpreted the data with assistance from C.M and Z.A.K. C.M and Z.A.K supervised the project.

Acknowledgements

We would like to thank Hannes Wydler for all of his technical assistance during this project. We would also like to thank Lukas Huber at EMPA Dübendorf for performing the water sorption measurements. R.O.D, Z.A.K, D.B and J.F acknowledge support for this work from SNF grant # 200021_156581.

Appendix A1

The volume of water required to hydroxylate the particles (V_w) was calculated as:

$$V_w = \frac{m_{SiO_2} \cdot A_s \cdot \sigma_{SiOH} \cdot M_w}{\rho_W \cdot N_A} \quad \text{(A1)}$$

where m_{SiO_2} is the mass of silica particles, A_s is the specific surface area of the silica particles, σ_{SiOH} = 4.6 nm^{-2} is the desired concentration of surface silanol groups following (Zhuralev, 2000), M_w is the molar mass of water, ρ_w is the density of water and N_A is the Avogadro constant. The amount of organosilane added to methylate the particles was calculated following Eq. A1 except that M_O and ρ_O are molar mass and the density of the respective organosilane.

$$V_O = \frac{m_{SiO_2} \cdot A_s \cdot \sigma_{SiOH} \cdot M_O}{\rho_O \cdot N_A} \quad \text{(A2)}$$

The *AF* curves of the hydroxylated and methylated samples are shown in Figures A1 and A2.

Appendix A2

Ice crystal growth in ZINC for a given residence time (t), supersaturation with respect to ice (S_i) and temperature (T) was calculated based on Rogers and Yau (1989) and Lohmann et al. (2016) as follows:

$$r(t, S_i, T) = \sqrt{r_0^2 + 2\alpha \left(\frac{S_i - 1}{F_k + F_D}\right) t} \quad \text{(A3)}$$

where $r(t, S_i, T)$ is the final radius of a spherical ice crystal. A spherical assumption for ice crystals is based on ~~observations that small ice crystals formed on spherical particles are spherical~~the small size of the ice crystals detected in this study (~1 µm) and the fact that the ice is growing on spherical particles (Harrington et al., 2019). r_0 represents the original radius of the silica

particles (400 nm) and is squared in the equation to account for the capacitance, which for spherical particles is equal to its radius (Rogers and Yau, 1989). α is the accommodation coefficient for water molecules to be incorporated into an ice lattice, which has been observed as ranging between 0.004 and ~~0.1 or 0.~~21 for the temperatures investigated in this study (Earle et al., 2010; Isono and Iwai, 1969; Magee et al., 2006; Skrotzki et al., 2013) and are chosen as 0.1 and 0.2 in this study. The terms in the denominator of Eq. A3 are:

$$F_k = \left(\frac{L_s}{R_v T} - 1\right)\frac{L_s}{KT} \quad \text{(A4)}$$

where L_s is the latent heat of sublimation as parameterized by Murphy and Koop (2005), R_v is the moist gas constant and K represents the thermal conductivity coefficient taken from Beard and Pruppacher, (1971).

$$F_D = \frac{R_v T}{D_v e_{s,i}(T)} \quad \text{(A5)}$$

Here the water vapour diffusion coefficient in air (D_v) was taken from Hall and Pruppacher, (1976) and $e_{s,i}(T)$ is the ice saturation vapour pressure as parameterized in Murphy and Koop, (2005).

For each experimental temperature, the S_i required for a crystal to grow to 1 μm, the ice threshold in the OPC, is calculated by reorganizing Eq. A3 and using a residence time of 10 s.

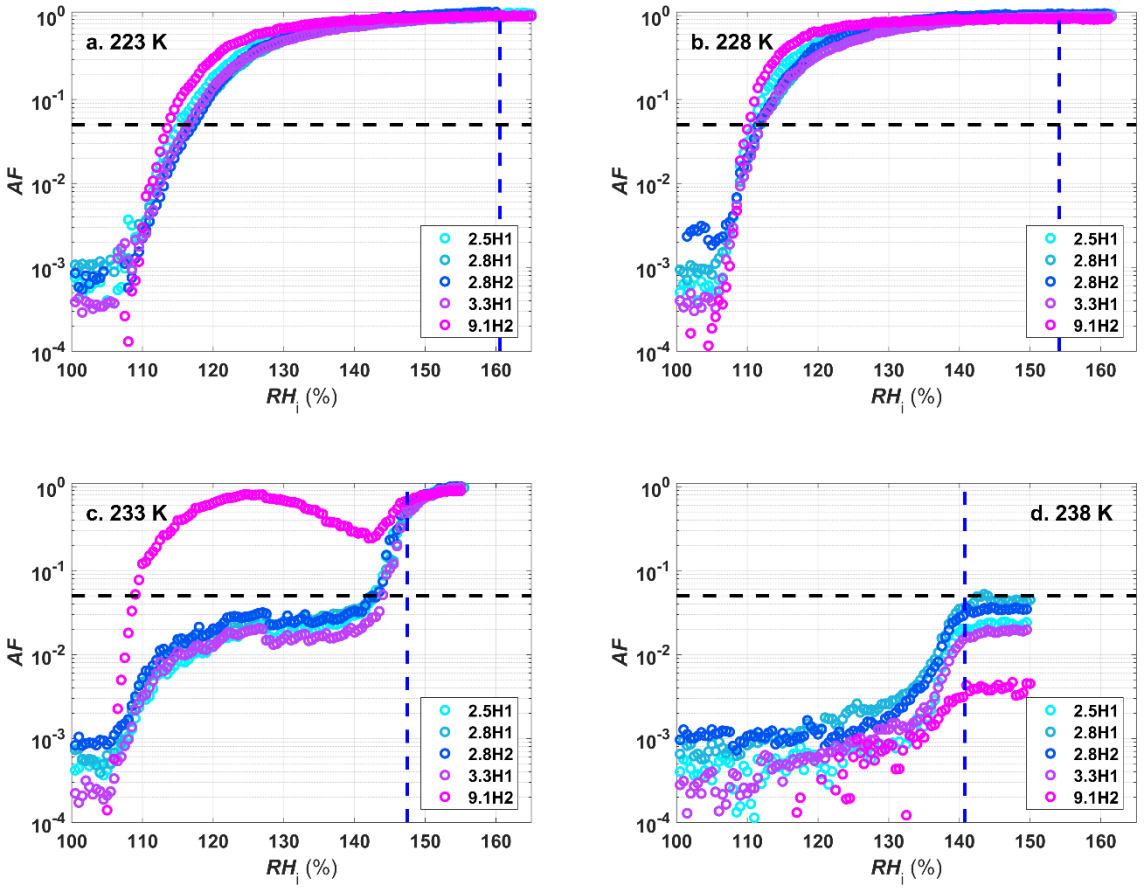

Figure A1: Activated Fraction (*AF*) curves for the porous hydroxylated samples as a function of RH_i at 223 K (panel a.), 228 K (panel b.), 233 K (panel c.) and 238 K (panel d.). The blue dashed vertical line represents the RH_i corresponding to water saturation. The black dashed horizontal line indicates the $AF_{0.05}$ threshold. The decrease in AF for the 9.1H2 sample (magenta circles) in panel c was reproducible but disappeared at 231 K (not shown).

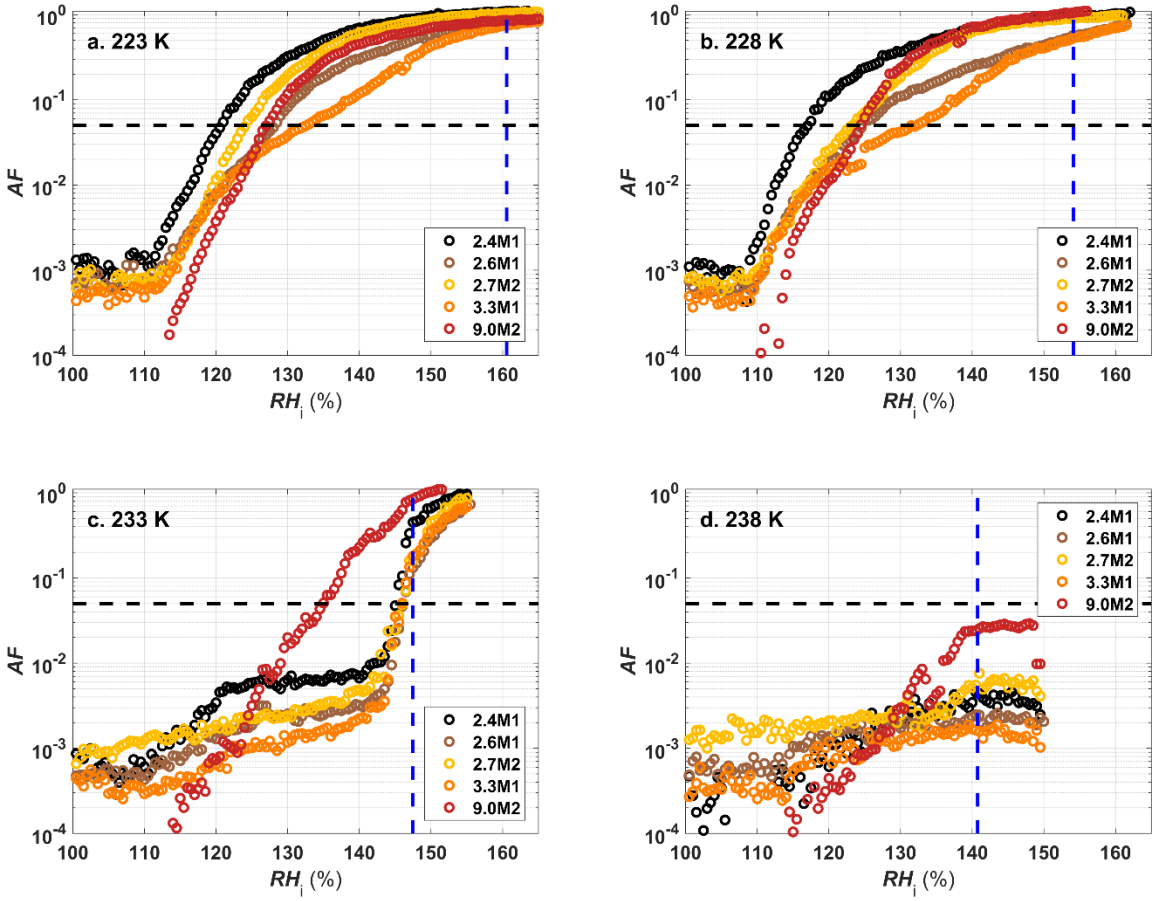

Figure A2: Activated Fraction (*AF*) curves for the methylated samples as a function of RH_i at 223 K (panel a.), 228 K (panel b.), 233 K (panel c.) and 238 K (panel d.). The blue dashed vertical line represents the RH_i corresponding to water saturation. The black dashed horizontal line indicates the $AF_{0.05}$ threshold.

3.5 References

Atkinson, J. D., Murray, B. J. and O'Sullivan, D.: Rate of Homogenous Nucleation of Ice in Supercooled Water, J. Phys. Chem. A, 120(33), 6513–6520, doi:10.1021/acs.jpca.6b03843, 2016.

Bartels-Rausch, T., Jacobi, H.-W., Kahan, T. F., Thomas, J. L., Thomson, E. S., Abbatt, J. P. D., Ammann, M., Blackford, J. R., Bluhm, H., Boxe, C., Domine, F., Frey, M. M., Gladich, I., Guzmán, M. I., Heger, D., Huthwelker, T., Klán, P., Kuhs, W. F., Kuo, M. H., Maus, S., Moussa, S. G., McNeill, V. F., Newberg, J. T., Pettersson, J. B. C., Roeselová, M. and Sodeau, J. R.: A review of air–ice chemical and physical interactions (AICI): liquids, quasi-liquids, and solids in snow, Atmospheric Chem. Phys., 14(3), 1587–1633, doi:https://doi.org/10.5194/acp-14-1587-2014, 2014.

Bassett, D. R., Boucher, E. A. and Zettlemoyer, A. C.: Adsorption studies on ice-nucleating substrates. Hydrophobed silicas and silver iodide, J. Colloid Interface Sci., 34(3), 436–446, doi:10.1016/0021-9797(70)90203-1, 1970.

Beard, K. V. and Pruppacher, H. R.: A Wind Tunnel Investigation of the Rate of Evaporation of Small Water Drops Falling at Terminal Velocity in Air, J. Atmospheric Sci., 28(8), 1455–1464, doi:10.1175/1520-0469(1971)028<1455:AWTIOT>2.0.CO;2, 1971.

Beck, J. S., Vartuli, J. C., Roth, W. J., Leonowicz, M. E., Kresge, C. T., Schmitt, K. D., Chu, C. T. W., Olson, D. H., Sheppard, E. W. and McCullen, S. B.: A new family of mesoporous molecular sieves prepared with liquid crystal templates, J. Am. Chem. Soc., 114(27), 10834–10843, 1992.

Bergna, H. E.: Colloid Chemistry of Silica, in The Colloid Chemistry of Silica, vol. 234, pp. 1–47, American Chemical Society., 1994.

Bhambhani, M. R., Cutting, P. A., Sing, K. S. W. and Turk, D. H.: Analysis of nitrogen adsorption isotherms on porous and nonporous silicas by the BET and αs methods, J. Colloid Interface Sci., 38(1), 109–117, doi:10.1016/0021-9797(72)90226-3, 1972.

Boose, Y., Kanji, Z. A., Kohn, M., Sierau, B., Zipori, A., Crawford, I., Lloyd, G., Bukowiecki, N., Herrmann, E., Kupiszewski, P., Steinbacher, M. and Lohmann, U.: Ice Nucleating Particle Measurements at 241 K during Winter Months at 3580 m MSL in the Swiss Alps, J. Atmospheric Sci., 73(5), 2203–2228, doi:10.1175/JAS-D-15-0236.1, 2016.

Broekhoff, J. C. P. and de Boer, J. H.: Studies on pore systems in catalysts: IX. Calculation of pore distributions from the adsorption branch of nitrogen sorption isotherms in the case of open cylindrical pores A. Fundamental equations, J. Catal., 9(1), 8–14, doi:10.1016/0021-9517(67)90174-1, 1967.

Brunauer, S., Emmett, P. H. and Teller, E.: Adsorption of gases in multimolecular layers, J. Am. Chem. Soc., 60(2), 309–319, 1938.

Burkert-Kohn, M., Wex, H., Welti, A., Hartmann, S., Grawe, S., Hellner, L., Herenz, P., Atkinson, J. D., Stratmann, F. and Kanji, Z. A.: Leipzig Ice Nucleation chamber Comparison (LINC): intercomparison of four online ice nucleation counters, Atmos Chem Phys, 17(18), 11683–11705, doi:10.5194/acp-17-11683-2017, 2017.

Campbell, J. M. and Christenson, H. K.: Nucleation- and Emergence-Limited Growth of Ice from Pores, Phys. Rev. Lett., 120(16), 165701, doi:10.1103/PhysRevLett.120.165701, 2018.

Campbell, J. M., Meldrum, F. C. and Christenson, H. K.: Is Ice Nucleation from Supercooled Water Insensitive to Surface Roughness?, J. Phys. Chem. C, 119(2), 1164–1169, doi:10.1021/jp5113729, 2015.

Campbell, J. M., Meldrum, F. C. and Christenson, H. K.: Observing the formation of ice and organic crystals in active sites, Proc. Natl. Acad. Sci., 114(5), 810–815, 2017.

Chen, J., Li, Q., Xu, R. and Xiao, F.: Distinguishing the Silanol Groups in the Mesoporous Molecular Sieve MCM-41, Angew. Chem. Int. Ed. Engl., 34(23–24), 2694–2696, doi:10.1002/anie.199526941, 1996.

Christenson, H. K.: Two-step crystal nucleation via capillary condensation, CrystEngComm, 15(11), 2030, doi:10.1039/c3ce26887j, 2013.

Cooper, W. A.: A Possible Mechanism for Contact Nucleation, J. Atmospheric Sci., 31(7), 1832–1837, doi:10.1175/1520-0469(1974)031<1832:APMFCN>2.0.CO;2, 1974.

David, R. O., Marcolli, C., Fahrni, J., Qiu, Y., Sirkin, Y. A. P., Molinero, V., Mahrt, F., Brühwiler, D., Lohmann, U. and Kanji, Z. A.: Pore condensation and freezing is responsible for ice formation below water saturation for porous particles, Proc. Natl. Acad. Sci., 116(17), 8184–8189, doi:10.1073/pnas.1813647116, 2019.

Deschamps, J., Audonnet, F., Brodie-Linder, N., Schoeffel, M. and Alba-Simionesco, C.: A thermodynamic limit of the melting/freezing processes of water under strongly hydrophobic nanoscopic confinement, Phys Chem Chem Phys, 12(7), 1440–1443, doi:10.1039/B920816J, 2010.

Earle, M. E., Kuhn, T., Khalizov, A. F. and Sloan, J. J.: Volume nucleation rates for homogeneous freezing in supercooled water microdroplets: results from a combined experimental and modelling approach, Atmospheric Chem. Phys., 10(16), 7945–7961, doi:https://doi.org/10.5194/acp-10-7945-2010, 2010.

Findenegg, G. H., Jähnert, S., Akcakayiran, D. and Schreiber, A.: Freezing and Melting of Water Confined in Silica Nanopores, ChemPhysChem, 9(18), 2651–2659, doi:10.1002/cphc.200800616, 2008.

Fletcher, N. H.: The physics of rainclouds, Cambridge University Press., 1962.

Fletcher, N. H.: Active Sites and Ice Crystal Nucleation, J. Atmospheric Sci., 26(6), 1266–1271, doi:10.1175/1520-0469(1969)026<1266:ASAICN>2.0.CO;2, 1969.

Fukuta, N.: Activation of Atmospheric Particles as Ice Nuclei in Cold and Dry Air, J. Atmospheric Sci., 23(6), 741–750, doi:10.1175/1520-0469(1966)023<0741:AOAPAI>2.0.CO;2, 1966.

Garimella, S., Rothenberg, D. A., Wolf, M. J., David, R. O., Kanji, Z. A., Wang, C., Rösch, M. and Cziczo, D. J.: Uncertainty in counting ice nucleating particles with continuous flow diffusion chambers, Atmos Chem Phys, 17(17), 10855–10864, doi:10.5194/acp-17-10855-2017, 2017.

Hall, W. D. and Pruppacher, H. R.: The Survival of Ice Particles Falling from Cirrus Clouds in Subsaturated Air, J. Atmospheric Sci., 33(10), 1995–2006, doi:10.1175/1520-0469(1976)033<1995:TSOIPF>2.0.CO;2, 1976.

Hamadeh, I. M., Yeboah, S. A., Trumbull, K. A. and Griffiths, P. R.: Preparation of Calibration Standards for Quantitative Diffuse Reflectance Infrared Spectrometry, Appl. Spectrosc., 38(4), 486–491, 1984.

Harrington, J. Y., Moyle, A., Hanson, L. E. and Morrison, H.: On Calculating Deposition Coefficients and Aspect-Ratio Evolution in Approximate Models of Ice Crystal Vapor Growth, J. Atmospheric Sci., 76(6), 1609–1625, doi:10.1175/JAS-D-18-0319.1, 2019.

Higuchi, K. and Fukuta, N.: Ice in the Capillaries of Solid Particles and its Effect on their Nucleating Ability, J. Atmospheric Sci., 23(2), 187–190, doi:10.1175/1520-0469(1966)023<0187:IITCOS>2.0.CO;2, 1966.

Ickes, L., Welti, A., Hoose, C. and Lohmann, U.: Classical nucleation theory of homogeneous freezing of water: thermodynamic and kinetic parameters, Phys. Chem. Chem. Phys. PCCP, 17(8), 5514–5537, doi:10.1039/c4cp04184d, 2015.

Isono, K. and Iwai, K.: Growth Mode of Ice Crystals in Air at Low Pressure, Nature, 223(5211), 1149–1150, doi:10.1038/2231149a0, 1969.

Jähnert, S., Vaca Chávez, F., Schaumann, G. E., Schreiber, A., Schönhoff, M. and Findenegg, G. H.: Melting and freezing of water in cylindrical silica nanopores, Phys. Chem. Chem. Phys., 10(39), 6039, doi:10.1039/b809438c, 2008.

Kanji, Z. A., Florea, O. and Abbatt, J. P. D.: Ice formation via deposition nucleation on mineral dust and organics: dependence of onset relative humidity on total particulate surface area, Environ. Res. Lett., 3(2), 025004, doi:10.1088/1748-9326/3/2/025004, 2008.

Kanji, Z. A., Welti, A., Chou, C., Stetzer, O. and Lohmann, U.: Laboratory studies of immersion and deposition mode ice nucleation of ozone aged mineral dust particles, Atmos Chem Phys, 13(17), 9097–9118, doi:10.5194/acp-13-9097-2013, 2013.

Kaufmann, L., Marcolli, C., Luo, B. and Peter, T.: Refreeze experiments with water droplets containing different types of ice nuclei interpreted by classical nucleation theory, Atmos Chem Phys, 17(5), 3525–3552, doi:10.5194/acp-17-3525-2017, 2017.

Ketcham, W. M. and Hobbs, P. V.: An experimental determination of the surface energies of ice, Philos. Mag., 19(162), 1161–1173, doi:10.1080/14786436908228641, 1969.

Kiselev, A., Bachmann, F., Pedevilla, P., Cox, S. J., Michaelides, A., Gerthsen, D. and Leisner, T.: Active sites in heterogeneous ice nucleation—the example of K-rich feldspars, Science, 355(6323), 367–371, doi:10.1126/science.aai8034, 2017.

Kittaka, S., Ueda, Y., Fujisaki, F., Iiyama, T. and Yamaguchi, T.: Mechanism of freezing of water in contact with mesoporous silicas MCM-41, SBA-15 and SBA-16: role of boundary water of pore outlets in freezing, Phys. Chem. Chem. Phys., 13(38), 17222, doi:10.1039/c1cp21458f, 2011.

Kocherbitov, V. and Alfredsson, V.: Hydration of MCM-41 Studied by Sorption Calorimetry, J. Phys. Chem. C, 111(35), 12906–12913, doi:10.1021/jp072474r, 2007.

Koop, T.: Crystals creeping out of cracks, Proc. Natl. Acad. Sci., 114(5), 797–799, doi:10.1073/pnas.1620084114, 2017.

Koop, T. and Murray, B. J.: A physically constrained classical description of the homogeneous nucleation of ice in water, J. Chem. Phys., 145(21), 211915, doi:10.1063/1.4962355, 2016.

Koop, T., Luo, B., Tsias, A. and Peter, T.: Water activity as the determinant for homogeneous ice nucleation in aqueous solutions, Nature, 406(6796), 611–614, doi:10.1038/35020537, 2000.

Kovács, T. and Christenson, H. K.: A two-step mechanism for crystal nucleation without supersaturation, Faraday Discuss., 159(0), 123–138, doi:10.1039/C2FD20053H, 2012.

Kovács, T., Meldrum, F. C. and Christenson, H. K.: Crystal Nucleation without Supersaturation, J. Phys. Chem. Lett., 3(12), 1602–1606, doi:10.1021/jz300450g, 2012.

Kruk, M., Jaroniec, M. and Sayari, A.: Application of Large Pore MCM-41 Molecular Sieves To Improve Pore Size Analysis Using Nitrogen Adsorption Measurements, Langmuir, 13(23), 6267–6273, doi:10.1021/la970776m, 1997.

Kuhs, W. F., Sippel, C., Falenty, A. and Hansen, T. C.: Extent and relevance of stacking disorder in "ice Ic," Proc. Natl. Acad. Sci., 109(52), 21259–21264, doi:10.1073/pnas.1210331110, 2012.

Kumar, A., Marcolli, C., Luo, B. and Peter, T.: Ice nucleation activity of silicates and aluminosilicates in pure water and aqueous solutions – Part 1: The K-feldspar microcline, Atmospheric Chem. Phys., 18(10), 7057–7079, doi:https://doi.org/10.5194/acp-18-7057-2018, 2018.

Landers, J., Gor, G. Yu. and Neimark, A. V.: Density functional theory methods for characterization of porous materials, Colloids Surf. Physicochem. Eng. Asp., 437, 3–32, doi:10.1016/j.colsurfa.2013.01.007, 2013.

Linton, P., Rennie, A. R., Zackrisson, M. and Alfredsson*, V.: In Situ Observation of the Genesis of Mesoporous Silica SBA-15: Dynamics on Length Scales from 1 nm to 1 μm, Langmuir, 25(8), 4685–4691, doi:10.1021/la803543z, 2009a.

Linton, P., Hernandez-Garrido, J.-C., Midgley, P. A., Wennerström, H. and Alfredsson, V.: Morphology of SBA-15-directed by association processes and surface energies, Phys. Chem. Chem. Phys., 11(46), 10973–10982, doi:10.1039/B913755F, 2009b.

L. Malkin, T., J. Murray, B., G. Salzmann, C., Molinero, V., J. Pickering, S. and F. Whale, T.: Stacking disorder in ice I, Phys. Chem. Chem. Phys., 17(1), 60–76, doi:10.1039/C4CP02893G, 2015.

Lohmann, U., Lüönd, F. and Mahrt, F.: An Introduction to Clouds: From the Microscale to Climate, Camb. Core, doi:10.1017/CBO9781139087513, 2016.

Lupi, L., Hudait, A., Peters, B., Grünwald, M., Mullen, R. G., Nguyen, A. H. and Molinero, V.: Role of stacking disorder in ice nucleation, Nature, 551(7679), nature24279, doi:10.1038/nature24279, 2017.

Magee, N., Moyle, A. M. and Lamb, D.: Experimental determination of the deposition coefficient of small cirrus-like ice crystals near −50°C, Geophys. Res. Lett., 33(17), doi:10.1029/2006GL026665, 2006.

Mahrt, F., Marcolli, C., David, R. O., Grönquist, P., Meier, B., J, E., Lohmann, U. and Kanji, Z. A.: Ice nucleation abilities of soot particles determined with the Horizontal Ice Nucleation Chamber, Atmospheric Chem. Phys. Discuss., 1–41, doi:https://doi.org/10.5194/acp-2018-557, 2018.

Mahrt, F., Alpert, P. A., Dou, J., Grönquist, P., Arroyo, P. C., Ammann, M., Lohmann, U. and Kanji, Z. A.: Aging induced changes in ice nucleation activity of combustion aerosol as determined by near edge X-ray absorption fine structure (NEXAFS) spectroscopy, Environ. Sci. Process. Impacts, 22(4), 895–907, doi:10.1039/C9EM00525K, 2020a.

Mahrt, F., Kilchhofer, K., Marcolli, C., Grönquist, P., David, R. O., Rösch, M., Lohmann, U. and Kanji, Z. A.: The Impact of Cloud Processing on the Ice Nucleation Abilities of Soot Particles at Cirrus Temperatures, J. Geophys. Res. Atmospheres, 125(3), e2019JD030922, doi:10.1029/2019JD030922, 2020b.

Marcolli, C.: Deposition nucleation viewed as homogeneous or immersion freezing in pores and cavities, Atmos Chem Phys, 14(4), 2071–2104, doi:10.5194/acp-14-2071-2014, 2014.

Marcolli, C.: Technical note: Fundamental aspects of ice nucleation via pore condensation and freezing including Laplace pressure and growth into macroscopic ice, Atmospheric Chem. Phys., 20(5), 3209–3230, doi:https://doi.org/10.5194/acp-20-3209-2020, 2020.

Marcolli, C., Gedamke, S., Peter, T. and Zobrist, B.: Efficiency of immersion mode ice nucleation on surrogates of mineral dust, Atmos Chem Phys, 7(19), 5081–5091, doi:10.5194/acp-7-5081-2007, 2007.

McFarquhar, G. M., Baumgardner, D. and Heymsfield, A. J.: Background and Overview, Meteorol. Monogr., 58, v–ix, doi:10.1175/AMSMONOGRAPHS-D-16-0018.1, 2017.

Miyahara, M., Kanda, H., Yoshioka, T. and Okazaki, M.: Modeling Capillary Condensation in Cylindrical Nanopores: A Molecular Dynamics Study, Langmuir, 16(9), 4293–4299, doi:10.1021/la991227e, 2000.

Moore, E. B., de la Llave, E., Welke, K., Scherlis, D. A. and Molinero, V.: Freezing, melting and structure of ice in a hydrophilic nanopore, Phys. Chem. Chem. Phys., 12(16), 4124, doi:10.1039/b919724a, 2010.

Moore, E. B., Allen, J. T. and Molinero, V.: Liquid-Ice Coexistence below the Melting Temperature for Water Confined in Hydrophilic and Hydrophobic Nanopores, J. Phys. Chem. C, 116(13), 7507–7514, doi:10.1021/jp3012409, 2012.

Morishige, K., Yasunaga, H. and Uematsu, H.: Stability of Cubic Ice in Mesopores, J. Phys. Chem. C, 113(8), 3056–3061, doi:10.1021/jp8088935, 2009.

Mülmenstädt, J., Sourdeval, O., Delanoë, J. and Quaas, J.: Frequency of occurrence of rain from liquid-, mixed-, and ice-phase clouds derived from A-Train satellite retrievals: RAIN FROM LIQUID- AND ICE-PHASE CLOUDS, Geophys. Res. Lett., 42(15), 6502–6509, doi:10.1002/2015GL064604, 2015.

Murphy, D. M. and Koop, T.: Review of the vapour pressures of ice and supercooled water for atmospheric applications, Q. J. R. Meteorol. Soc., 131(608), 1539–1565, doi:10.1256/qj.04.94, 2005.

Murray, B. J., L. Broadley, S., W. Wilson, T., J. Bull, S., H. Wills, R., K. Christenson, H. and J. Murray, E.: Kinetics of the homogeneous freezing of water, Phys. Chem. Chem. Phys., 12(35), 10380–10387, doi:10.1039/C003297B, 2010.

Muster, T. H., Prestidge, C. A. and Hayes, R. A.: Water adsorption kinetics and contact angles of silica particles, Colloids Surf. Physicochem. Eng. Asp., 176(2), 253–266, 2001.

Nichman, L., Wolf, M., Davidovits, P., Onasch, T. B., Zhang, Y., Worsnop, D. R., Bhandari, J., Mazzoleni, C. and Cziczo, D. J.: Laboratory study of the heterogeneous ice nucleation on black-carbon-containing aerosol, Atmospheric Chem. Phys., 19(19), 12175–12194, doi:https://doi.org/10.5194/acp-19-12175-2019, 2019.

Pach, E. and Verdaguer, A.: Pores Dominate Ice Nucleation on Feldspars, J. Phys. Chem. C, 123(34), 20998–21004, doi:10.1021/acs.jpcc.9b05845, 2019.

Page, A. J. and Sear, R. P.: Heterogeneous Nucleation in and out of Pores, Phys. Rev. Lett., 97(6), doi:10.1103/PhysRevLett.97.065701, 2006.

Pedevilla, P., Fitzner, M. and Michaelides, A.: What makes a good descriptor for heterogeneous ice nucleation on OH-patterned surfaces, Phys. Rev. B, 96(11), 115441, doi:10.1103/PhysRevB.96.115441, 2017.

Pruppacher, H. R. and Klett, J. D.: Microphysics of Clouds and Precipitation, Kluwer Academic Publishers. [online] Available from: http://www.springer.com/de/book/9780792342113 (Accessed 30 May 2017), 1997.

Riechers, B., Wittbracht, F., H?tten, A. and Koop, T.: The homogeneous ice nucleation rate of water droplets produced in a microfluidic device and the role of temperature uncertainty, Phys. Chem. Chem. Phys., 15(16), 5873, doi:10.1039/c3cp42437e, 2013.

Rogers, R. R. and Yau, M. K.: A short course in cloud physics, 3rd ed., Pergamon Press, Oxford., 1989.

Salazar, I. and Sepúlveda, L.: Nucleation of water by hydrophobic silicas, J. Colloid Interface Sci., 94(1), 70–74, doi:10.1016/0021-9797(83)90235-7, 1983.

Schreiber, A., Ketelsen, I. and Findenegg, G. H.: Melting and freezing of water in ordered mesoporous silica materials, Phys. Chem. Chem. Phys., 3(7), 1185–1195, doi:10.1039/B010086M, 2001.

Seinfeld, J. H., Bretherton, C., Carslaw, K. S., Coe, H., DeMott, P. J., Dunlea, E. J., Feingold, G., Ghan, S., Guenther, A. B., Kahn, R., Kraucunas, I., Kreidenweis, S. M., Molina, M. J., Nenes, A., Penner, J. E., Prather, K. A., Ramanathan, V., Ramaswamy, V., Rasch, P. J., Ravishankara, A. R., Rosenfeld, D., Stephens, G. and Wood, R.: Improving our fundamental

understanding of the role of aerosol−cloud interactions in the climate system, Proc. Natl. Acad. Sci., 113(21), 5781–5790, doi:10.1073/pnas.1514043113, 2016.

Sing, K. S. W.: Reporting physisorption data for gas/solid systems with special reference to the determination of surface area and porosity (Recommendations 1984), Pure Appl. Chem., 57(4), 603–619, doi:10.1351/pac198557040603, 2009.

Skrotzki, J., Connolly, P., Schnaiter, M., Saathoff, H., Möhler, O., Wagner, R., Niemand, M., Ebert, V. and Leisner, T.: The accommodation coefficient of water molecules on ice – cirrus cloud studies at the AIDA simulation chamber, Atmos Chem Phys, 13(8), 4451–4466, doi:10.5194/acp-13-4451-2013, 2013.

Stetzer, O., Baschek, B., Lüönd, F. and Lohmann, U.: The Zurich Ice Nucleation Chamber (ZINC)-A New Instrument to Investigate Atmospheric Ice Formation, Aerosol Sci. Technol., 42(1), 64–74, doi:10.1080/02786820701787944, 2008.

Thommes, M., Kaneko, K., Neimark, A. V., Olivier, J. P., Rodriguez-Reinoso, F., Rouquerol, J. and Sing, K. S. W.: Physisorption of gases, with special reference to the evaluation of surface area and pore size distribution (IUPAC Technical Report), Pure Appl. Chem., 87(9–10), 1051–1069, doi:10.1515/pac-2014-1117, 2015.

Umo, N. S., Wagner, R., Ullrich, R., Kiselev, A., Saathoff, H., Weidler, P. G., Cziczo, D. J., Leisner, T. and Möhler, O.: Enhanced ice nucleation activity of coal fly ash aerosol particles initiated by ice-filled pores, Atmospheric Chem. Phys., 19(13), 8783–8800, doi:https://doi.org/10.5194/acp-19-8783-2019, 2019.

Vali, G., DeMott, P. J., Möhler, O. and Whale, T. F.: Technical Note: A proposal for ice nucleation terminology, Atmospheric Chem. Phys., 15(18), 10263–10270, doi:10.5194/acp-15-10263-2015, 2015.

Wagner, R., Kiselev, A., Möhler, O., Saathoff, H. and Steinke, I.: Pre-activation of ice-nucleating particles by the pore condensation and freezing mechanism, Atmos Chem Phys, 16(4), 2025–2042, doi:10.5194/acp-16-2025-2016, 2016.

Wang, B., Knopf, D. A., China, S., Arey, B. W., Harder, T. H., Gilles, M. K. and Laskin, A.: Direct observation of ice nucleation events on individual atmospheric particles, Phys. Chem. Chem. Phys., 18(43), 29721–29731, doi:10.1039/C6CP05253C, 2016.

Wang, J., Xue, H., Zhou, B., Yao, Y.-F. and Hansen, E. W.: Interfacial water in mesopores and its implications to the surface features – A solid state NMR study, Appl. Surf. Sci., 484, 1154–1160, doi:10.1016/j.apsusc.2019.04.095, 2019.

Zhuravlev, L. T.: The surface chemistry of amorphous silica. Zhuravlev model, Colloids Surf. Physicochem. Eng. Asp., 173(1), 1–38, 2000.

Zobrist, B., Koop, T., Luo, B. P., Marcolli, C. and Peter, T.: Heterogeneous Ice Nucleation Rate Coefficient of Water Droplets Coated by a Nonadecanol Monolayer, J. Phys. Chem. C, 111(5), 2149–2155, doi:10.1021/jp066080w, 2007.

Reviewer comments are reproduced in bold and the author responses are in regular typeface. All line numbers in the authors' response refer to the revised manuscript. New text added to the manuscript in italics.

Interactive comment on "The Role of Contact Angle and Pore Width on Pore Condensation and Freezing" by Robert O. David et al.

Anonymous Referee #1

David et al. present ice nucleation measurements with well-characterized porous silica particles to investigate the efficiency of the pore condensation and freezing (PCF) ice formation pathway as a function of the particles' pore diameter, contact angle, and surface functionalization. The reported ice nucleation behavior is generally in agreement with that predicted by the inverse Kelvin equation, which is the starting point to theoretically describe the PCF mechanism. In some cases, further considerations, like limited growth time of ice crystals in the ZINC CFDC and pressure-dependent homogeneous ice nucleation rates, were taken into account to fully explain the experimental observations. It therefore remains challenging to derive a general parameterization of the PCF mechanism for e.g. ambient dust particles, but the experiments presented in this manuscript with the synthesized particles are an important step to understand which factors control the ice nucleation behavior of porous particles. A particular strength of the study is the comprehensive characterization of the particles with a number of different techniques as presented in Sect. 3.1. The manuscript itself is well-structured and in most parts clearly written. Reading the discussion of the ice nucleation measurements, however, was sometimes a bit challenging due to the variety of explanations taken into account to reconcile the findings with theory. I suggest below a couple of points which would need further clarifications, but otherwise recommend the publication of this article in ACP.

We thank the reviewer for the positive recommendation and for raising several points that we now address individually below and in the revised manuscript to make the paper clearer.

Specific comments:

1) Page 13, line 7: How did you exactly infer the range of contact angles for a given MCM-41 sample as also listed in Table 1 – did you use the uncertainty of d_DFT listed in Table 1, thus using e.g. pore diameters between 3 and 3.6 nm for the 3.3M1 sample in the calculation?

Indeed, we used the mean d_{DFT} and its uncertainty to report the spread in measured contact angles reported in Table 1 based on the humidity where the steepest condensation step was observed in the water sorption measurements. This has now been clarified on page 14 lines 7-8 by changing the sentence to read: "*The water contact angles for the MCM-41 particles ranged between 41˚- 45˚ and 75˚- 80˚, for the hydroxylated and methylated samples, respectively, based on the observed value and uncertainty (listed in Table 1) in the measured* d_{DFT}."

2) Page 13, line 12: Concerning the difficulty in the assignment of the "correct pore diameter responsible for the *initial* pore condensation": This statement seems to me a bit in contradiction with the one on page 6, line 14/15, saying that you did not use the onset relative humidity in the water sorption isotherms to compute the contact angle but the value where the pore condensation step is the steepest. So, the average pore diameters listed in Table 1 should be a reasonable choice for the computation and not the lowest value of e.g. 7 nm for the SBA-15 samples.

Table 1 represent the bulk properties of the particles, which in this case would be representative of the majority of the pores within the particles. The narrow pore size distribution of the MCM-41 particles, allows for the steepest condensation step in the sorption measurements to be representative of the

majority of the pores, especially when the uncertainty in d_{DFT} is considered. Indeed, the uncertainty in d_{DFT} accounted for in Table 1 and a range of possible contact angles is reported for all of the samples that underwent sorption measurements. However, as the SBA-15 particles have a wide distribution in pore diameters (7 – 16 nm, see Fig. 2), the uncertainty in d_{DFT} (9 ±1.1 nm) is no longer enough to account for the range of possible pore sizes and corresponding contact angles. Furthermore, as the narrowest pores in the SBA-15 samples, which fill at lower humidities than their wider counterparts, are likely responsible for the observed freezing, it is necessary to obtain a larger range in contact angles for these particles. We have now added: "*based on the uncertainty in d_{DFT} alone (±1.1 nm)*", to the sentence to clarify this point on page 15 lines 1-2.

3) Page 14: I have a couple of questions regarding the DSC measurements: Is there an influence of external ice on the initiation of freezing in the pores (in the caption of Fig. 4 you use the expression "ice growth into pores"? Did you also record the DSC thermograms during heating, are the peak positions different from the cooling runs? How do your results compare with previous DSC measurements for MCM-41 and SBA-15 as e.g. summarized in Marcolli (2014)?

Indeed, ice grows into the pores from the frozen bulk water in the slurry. Thus, the freezing of pore water in DSC experiments is not determined by nucleation rates but by the melting point depression within pores, as is explained on page 15 lines 6-13. Unfortunately, the heat uptake during the warming cycle was undetectable for the smaller diameter pores and is therefore not shown. For the larger diameter pores, the heat release during freezing corresponds approximately with the heat uptake during melting considering the difference in enthalpy between freezing and melting. The observed freezing temperatures are in accordance with values reported in Fig. 1 of Marcolli (2014).

4) Page 16, line 22/23 & page 26, line 27: The reference to Skrotzki et al. (2013) does not agree with the choice of an accommodation coefficient as low as 0.1 to compute the ice growth. As far as I can see, Skrotzki et al. (2013) reported accommodation coefficients > 0.2 for all conducted experiments with an overall average value of 0.7. So, I am not fully convinced that the limited ice growth is the best explanation for the absence of immediate ice growth as soon as ice saturation is reached in ZINC.

The reviewer is correct in that the accommodation coefficient proposed by Skrotzki et al, (2013) are above 0.2. However, Skrotzki et al, (2013) also report values from previous studies that are as low as 0.004, therefore an accommodation coefficient of 0.1 is also realistic. We have now updated the citations to cover the complete range in values reported in the literature. The following citations have been added to the main text and in the appendix: Earle et al., (2010), Isono and Iwai, (1969) and Magee et al., (2006). Therefore, we still believe that a low accommodation coefficient is a valid explanation for the delayed onset and keep the lines for 0.2 and 0.1 as accommodation coefficients in Figure 6 and Figure 6, 7, and 8, respectively.

The authors discuss on page 17 that a non-negligible fraction of the aerosol might experience a lower supersaturation than computed for the center of the aerosol lamina in the CFDC - this might also explain in part the higher onset values for ice growth on the 2.8C2 and 2.8H2 particles.

Yet, we agree with the reviewer that a low accommodation coefficient is not the only possible explanation for the absence of immediate ice growth. The increase in humidity above 100% for first ice crystal detection could also be due to the initial ice growth out of the pores being stacking disordered. As has been shown in molecular dynamic simulations, initial ice nucleation and ice in confinement is typically stacking disordered (e.g. Lupi et al., 2017; Moore et al., 2010). Stacking disordered ice requires a higher humidity to be stable than bulk ice. As such, a higher humidity would be required for the ice to initially grow. However, once the first few monolayers of ice covers the particle surface, ice growth likely transitions to hexagonal ice. If this transition takes longer than some seconds, ice growth within ZINC would require supersaturation with respect to bulk ice, since the growth is occurring on stacking disordered ice. Additionally, it is possible that some of the particles are exposed to lower humidities than expected, if they are traveling outside of the lamina (Garimella et al., 2017). However, this effect is more relevant at higher humidities when the gradient in temperature between the cold and warm wall is higher. Therefore, we do not expect this to be a major issue at these low humidities.

Also, the onset RHi values are given for an already quite high ice-active fraction of 5%. In the full ZINC scans for 2.8H2 in Fig. A1 a and b one can see that the ice growth initiates clearly below 110% RHi – so not too far from the expected value of 100% RHi if also considering the RHi uncertainty in ZINC.

Indeed, as mentioned by the reviewer, at these humdities, the uncertainty due to the temperature reported by the thermocouples and thus the calculated relative humidity that the particles are exposed to (~ ± 5% RH_i) presents an additional uncertainty in our reported onsets. As such it is possible that the observed onsets (Fig. A1) could be occurring closer to ice saturation than we show considering the 5% uncertainty in RH_i. We revised the manuscript to discuss all these potential explanations in the text by stating the following:

"Moreover, the reported AF of 0.05 do not correspond with the ice onset. Considering Fig. A1, the initial ice is observed at RH_i 110 % and 108% for 223 and 228 K, respectively. Lupi et al., (2017) and Moore et al., (2010) have shown in MD studies that stacking disordered ice is formed in confinement and during nucleation, requiring a humidity higher than 100% to grow ice. Additionally, the calculated humidity that particles are exposed to in ZINC depends on the temperatures of the warm and cold walls, which are measured by thermocouples that have an uncertainty of ±0.1 K (Stetzer et al., 2008). *This uncertainty (±5 %) can lead to a higher reported humidity than required to observe ice nucleation and is included in the vertical error bars in Figure 6, 7 and 8."* on page 18 lines 22-29.

Did the particles enter ZINC in a dry air flow (without pre-condensed water in the pores) – could this also influence the ice nucleation measurements?

Additionally, we have now mentioned in the text that the particles were aerosolized and transported to ZINC using evaporated liquid nitrogen on page 8 lines 5-6.

5) Page 16, line 25 and page 26, line 24: The reference to Järvinen et al. (2016) also does not seem appropriate for me to justify a spherical shape of ice particles in the computations. They observed "quasi-spherical" ice crystals from the freezing of water droplets during strong

convection, which is a clearly different process from growth of ice crystals on near-spherical solid silica particles as in the present study.

We agree with the reviewer's opinion that the freezing and subsequent growth of supercooled droplets is likely a different process than the growth of ice on spherical aerosol particles. We have therefore changed the citation to Harrington et al., (2019), where it is assumed that at such small ice crystal sizes (~1 µm), the ice is spherical. We have now updated the sentence to read: *"The ice crystal shape in the growth calculation was assumed to be spherical due to the small final size (~1 µm) and its growth on spherical particles (Harrington et al., 2019)."* on page 18 lines 19-20.

6) Page 18, line 22ff, discussion related to the increase in the AF to 0.02 for the 2.8H2 sample up to RHi = 120%. I am a bit confused by this paragraph: In the preceding paper by David et al. (2019) in PNAS, the authors show in Fig. 2 the ZINC scans for porous MCM-41 particles with 3.8 nm pore diameter. This pore diameter should be large enough to host a critical ice germ at 233 K. But in the ZINC scan at -40◦C, ice formation did not occur below water saturation, and was explained by the fact that the homogeneous ice nucleation rates are not large enough to observe ice within the residence time of ZINC. If you applied the same argumentation with the pressure dependent parameterization of CNT as presented in the current manuscript, why didn't you detect any freezing signal for the 3.8 nm pore diameter particles at low RH? Could the small freezing signal for the 2.8H2 sample at lower RH not simply be due to immersion freezing within the pores? If I understood correctly, you used this explanation for the freezing signal observed for the 9.0M2 particles at 233 K (Fig. A2c and page 22, lines 24-27). The ZINC scan at 238 K with the 2.8H2 particles shows that at least the external particle surface contains active sites for condensation or immersion freezing (page 19, line 4/5). In contrast, the 3.8 nm pore diameter particles did not reveal a distinct immersion freezing signal at -35◦C (Fig. 2 in David et al., 2019).

The width of the pore size distribution and the dependence of nucleation rates and critical embryo size on CNT parameterization hamper the precise analysis of how freezing of pore water and growth out of pores depends on pore width and pore water volume. Because of these uncertainties, it is difficult to come to exact conclusions whether nucleation rates or pore diameter limit freezing within pores at 233 K. Applying a pressure dependent nucleation rate, ice in the 3.8 nm pores is expected to freeze at 233 K at negative pressures and within the residence time of ZINC, as the pores should be wide enough to host ice. However, since we did not observe freezing, the increase in the nucleation rate due to negative pressure is likely not the reason or counteracted by some other effect. We explain this in the following.

First, we consider immersion freezing as an alternative explanation for the weak freezing signal below water saturation for the sample 2.8H2 (see Fig. A1c). Yet even if there were nucleation sites within the pores, the DSC measurements indicate that the pores should be too narrow to host ice at 233 K (see Fig 5b) and the immersion sites are therefore, ineffective for ice nucleation. However, we cannot rule out that there are some pores large enough to accommodate the critical ice germ in the 2.5-2.8 nm samples where the freezing is not detectable in the DSC measurements. Indeed, the pore size distributions shown in Figure 2 indicate that these samples do have some pores larger than 3 nm in

diameter, which is close to the critical ice germ size at 233 K depending on the parametrization used (for example with the Murray et al, (2010) parametrization for hexagonal ice, the critical ice germ should be 2.9 nm at 233 K assuming a quasi-liquid layer of 0.38 nm). As such, it is possible that some pores in a small fraction of the particles are capable of supporting ice that freezes either homogeneously due to negative pressure or heterogeneously due to ice active sites within some of the pores. As to why we do not observe this freezing in the 3.8 nm samples used in David et al. (2019) we cannot fully isolate one reason. It may be because the particles in David et al. (2019) were not hydroxylated like the ones in this work (i.e. they were calcined), the water contact angle with the pore wall is expected to be higher. If this is the case, the pore fills at a higher relative humidity when the curvature of the pore water is less and the water would therefore experience a lower negative pressure in these wider pores, thus decreasing the homogeneous nucleation rate due to negative pressure in these pores. As the reviewer states, since the 3.8 nm samples did not exhibit any heterogeneous freezing ability (at T = 238 K) in David et al. (2019), then it is likely that no active sites exist in the pores even at 233 K. The combination of no active sites and a low nucleation rate from the lower negative pressure may be the reason no freezing was observed in the 3.8 nm samples in David et al. (2019).

7) Page 21, lines 5-13: See above, would a pressure dependent parameterization of CNT not also predict a strong increase in AF for the 3.8 nm pore diameter particles at 233 K and low RH? If you also plotted the active fraction curve for the 3.8 nm pore diameter particles at 233 K from David et al. (2019) into Fig. A1c (hydroxylated and calcined samples seem to behave rather similar, see Fig. 5), the 3.8 nm sample would not show an "intermediate" ice nucleation behavior between that of the 9 nm pore diameter and that of the 2.5 – 3.3 nm pore diameter particles, but just reveal a very low ice-active fraction until reaching water saturation. How would you interpret this difference?

Here again, the width of the pore size distribution and the dependence of nucleation rates and critical embryo size on CNT parameterization hamper a precise analysis. Comparing the pore size distribution of the 3.8 nm sample investigated in David et al. (2019, Fig.S5) and of 3.3H1 (Fig. 1b), there is a large overlap in pore diameters and especially the tail to large pores reaches for both samples up to 4.5 nm. If the pore width is limiting the stability of ice within pores, these pores indeed should behave similarly. However, as mentioned in the previous response, the negative pressure in the 3.8 nm pores in the samples from David et al, (2019) may differ even from the calcined samples (2.8C2) examined in this study due to the unstable nature of calcined samples depending on their age and exposure to water vapour (Muster et al., 2001). Therefore, it is not straightforward to extrapolate the results from the current study to those of David et al. (2019).

Minor comments and technical corrections:

1) Page 1, line 11: Maybe explicitly state "due to the inverse Kelvin effect"

We have now rephrased the sentence to state "*due to the inverse Kelvin effect*." (see page 1 line 13)

2) Page 1, line 14 + 17: Avoid the repetitive statements "play an important role in determining the relative humidity" and "play an important role in predicting the humidity" in the abstract.

Instead, you could also mention what type of chemical functionalization was employed and its effect on the ice nucleation behavior.

We remove the sentence referenced by the reviewer and shorten the sentence to read (see page 1 lines 16-18):

"*We find that for the pore diameters (2.2 – 9.2 nm) and water contact angles (15 – 78˚) covered in this study, our results reveal that the water contact angle plays an important role in predicting the humidity required for pore filling while the pore diameter determines the ability of pore water to freeze*."

3) Page 2, line 28: "is the interfacial energy"

Added, thanks.

4) Sect. 2.1.2: You should already indicate here the larger pore sizes of the SBA-15 particles compared to MCM-41.

We have now mentioned that larger pores were achieved using SBA-15 stating: "*To obtain larger pore diameters (~9 nm), SBA-15 particles (see Fig. 1c and d.) were synthesized similarly to Linton et al., (2009b) where*…" on page 4 line 18.

5) Page 5, line 4: Missing parenthesis ")" after "60◦C".

Added, thanks

6) Page 6, line 13/14: Could be phrased more clearly, you could also indicate the respective values for bulk water as a comparison.

We have rephrased the sentence to read "*For water in confinement at 25 ˚C, the values of* $\gamma(T)$ *and* $v_l(T)$ *are 71.69 mN/m and 20.5 m*^{3}*/mol, respectively (Kocherbitov and Alfredsson, 2007)."* on page 7 lines 9-10. We do not discuss the values for bulk water as it is beyond the scope of the current study.

7) Sect. 2.4: What was the relative humidity of the air before entering ZINC? Please indicate.

The humidity of the air entering ZINC is close to zero (< 1 %) as evaporated liquid nitrogen was used to aerosolize and transport the particles to ZINC. We have now clarified this in the text by stating: "…*supplied with evaporated liquid nitrogen (purity 6.0) to eliminate any residual humidity (RH < 1 % at 223 K)*…" on page 8 lines 5-6.

8) Fig. 1b & 2b: It is hard to discriminate the various bluish colors.

We thank the reviewer for pointing this out. We have now increased the resolution of the figure, which makes the color scheme more distinguishable (now Fig. 2b and 3b).

9) Page 12, line 4: You could also mention here in the text that you did a series of two adsorption/desorption cycles with the samples.

We have updated the text to read: "*Two water vapour sorption cycles were obtained for the samples 2.4M1, 2.5H1, 3.3M1, 3.3H1, 9.1H2 and 9.0M2 and the resultant isotherms are shown in Fig. 4*" on page 13 line 4-5.

10) Page 12, line 19: "The relative mass . . . does not return"

Corrected, thanks

11) Page 14, line 18: Maybe: "By contrast, the freezing temperature . . ."

We have updated the text to read: "*In contrast*,…" on page 15 line 20

12) Page 16, line 22: "peach" lines vs. "salmon" lines used in the caption of Fig. 5.

Thank you, we have updated to read "salmon" throughout the text**.**

13) Page 17, line 3 (second line in figure caption): Could you please briefly include the factors contributing to the RHi uncertainty in ZINC?

Thank you, we have now reworded the sentence to read: "*The error bars represent the maximum uncertainty in the calculated RH_i (±5 %) in ZINC arising from the uncertainty in the reported thermocouple temperature (±0.1 K; Stetzer et al., 2008) and encompass the standard deviation from averaging the experiments.*" in the figure caption

14) Page 17, line 9: "an AF_0.05"

Updated, thanks.

15) Page 21, line 25/26: Please check sentence structure.

We have updated the sentence to read: "*At 223 and 228 K, the samples with 2.4 nm pore diameter had the lowest $AF_{0.05}$ RH_i and the 3.3 nm particles the highest. The 2.6, 2.7, and 9.0 nm samples are in-between and overlap (Fig. 8)*." on page 23 lines 31-33.

16) Page 25, line 18 – 20: Please check sentence structure (avoid to use twice subclauses with "while").

Thank you for pointing this out. We have now split the sentence to read as follows: "*Therefore, ice nucleation parameterizations should be based on PCF below the HFT. Above the HFT, active sites present on the particle surface determine the ice nucleation activity at water saturation, while below water saturation active sites within pores are required to nucleate ice*." on page 27 lines 5-7.

Author References

Earle, M. E., Kuhn, T., Khalizov, A. F. and Sloan, J. J.: Volume nucleation rates for homogeneous freezing in supercooled water microdroplets: results from a combined experimental and modelling approach, Atmospheric Chem. Phys., 10(16), 7945–7961, doi:https://doi.org/10.5194/acp-10-7945-2010, 2010.

Garimella, S., Rothenberg, D. A., Wolf, M. J., David, R. O., Kanji, Z. A., Wang, C., Rösch, M. and Cziczo, D. J.: Uncertainty in counting ice nucleating particles with continuous flow diffusion chambers, Atmos Chem Phys, 17(17), 10855–10864, doi:10.5194/acp-17-10855-2017, 2017.

Harrington, J. Y., Moyle, A., Hanson, L. E. and Morrison, H.: On Calculating Deposition Coefficients and Aspect-Ratio Evolution in Approximate Models of Ice Crystal Vapor Growth, J. Atmospheric Sci., 76(6), 1609–1625, doi:10.1175/JAS-D-18-0319.1, 2019.

Isono, K. and Iwai, K.: Growth Mode of Ice Crystals in Air at Low Pressure, Nature, 223(5211), 1149–1150, doi:10.1038/2231149a0, 1969.

Kocherbitov, V. and Alfredsson, V.: Hydration of MCM-41 Studied by Sorption Calorimetry, J. Phys. Chem. C, 111(35), 12906–12913, doi:10.1021/jp072474r, 2007.

Linton, P., Hernandez-Garrido, J.-C., Midgley, P. A., Wennerström, H. and Alfredsson, V.: Morphology of SBA-15-directed by association processes and surface energies, Phys. Chem. Chem. Phys., 11(46), 10973–10982, doi:10.1039/B913755F, 2009.

Lupi, L., Hudait, A., Peters, B., Grünwald, M., Mullen, R. G., Nguyen, A. H. and Molinero, V.: Role of stacking disorder in ice nucleation, Nature, 551(7679), nature24279, doi:10.1038/nature24279, 2017.

Magee, N., Moyle, A. M. and Lamb, D.: Experimental determination of the deposition coefficient of small cirrus-like ice crystals near −50°C, Geophys. Res. Lett., 33(17), doi:10.1029/2006GL026665, 2006.

Moore, E. B., de la Llave, E., Welke, K., Scherlis, D. A. and Molinero, V.: Freezing, melting and structure of ice in a hydrophilic nanopore, Phys. Chem. Chem. Phys., 12(16), 4124, doi:10.1039/b919724a, 2010.

Murray, B. J., L. Broadley, S., W. Wilson, T., J. Bull, S., H. Wills, R., K. Christenson, H. and J. Murray, E.: Kinetics of the homogeneous freezing of water, Phys. Chem. Chem. Phys., 12(35), 10380–10387, doi:10.1039/C003297B, 2010.

Muster, T. H., Prestidge, C. A. and Hayes, R. A.: Water adsorption kinetics and contact angles of silica particles, Colloids Surf. Physicochem. Eng. Asp., 176(2), 253–266, 2001.

Stetzer, O., Baschek, B., Lüönd, F. and Lohmann, U.: The Zurich Ice Nucleation Chamber (ZINC)-A New Instrument to Investigate Atmospheric Ice Formation, Aerosol Sci. Technol., 42(1), 64–74, doi:10.1080/02786820701787944, 2008.

Reviewer comments are reproduced in bold and author responses are in regular typeface. All line numbers in the authors' response refer to the revised manuscript. Revised text is given in italics.

Review of "The Role of Contact Angle and Pore Width on Pore Condensation and Freezing," by R.O. David et al. 2019

Anonymous Referee #2

In their submitted manuscript, David et al. describe their attempts to utilize synthesized silica particles that have controlled surface pore widths, and alterations to those particles vis-a-vis functionalization, ´ to test the utility of pore condensation freezing as a physical parameterization for ice nucleation under certain atmospheric conditions. I am impressed by the detail and depth of the described studies and the submitted manuscript. However, I do feel that there remains room for improvement and clarity in an updated manuscript before acceptance for full publication in ACP. In particular, I suggest the authors strive to more clearly delineate where and when they think they can interpret their results purely on the basis of physical changes and where/when their understanding might be limited by the changes to the physical chemistry of the systems they are probing. In its current form the manuscript seeks to explain results primarily using physical parameters (i.e., size, geometry, bulk contact angle, etc.), but given the system (pore) sizes of exploration it might be that molecular-scale effects begin to play a role that cannot be dismissed.

Below I present an itemized list of thoughts and comments as I came to them in the text, which I hope put things into context. Following these comments I will return to some general items.

We thank the reviewer for the positive recommendation and for raising several points that we now address individually below and in the revised manuscript to make the paper clearer.

Itemized Scientific and Editorial Comments:

Specific Suggestions by Page and Line Number (page, line):

• (1,29) remove parentheses around (T)

Removed, thank you

• (1,30) I think it advisable to keep a more general definition of heterogeneous nucleation, like that of Vali et al. 1 . There he just says "nucleation aided by the presence of a foreign substance". "ice active site" could mean many things and does not necessarily give as general an impression.

We have reformulated to be consistent with the description provided by Vali et al. (2015*): At T > HFT ice formation takes place heterogeneously and is aided by the presence of a foreign substance (Fletcher, 1969; Kaufmann et al., 2017; Kiselev et al., 2017; Vali et al., 2015), which lowers the energy barrier required for the homogeneous nucleation of ice.*

• (2,7) The explanation of PCF that is when water "which can exist below water saturation in narrow pores" is confusing to me. Is it not that the local saturation condition is altered? In fact the pore water is at saturation, and this is why it condenses, it is simply not at bulk water saturation.

That is correct, as such we have revised the sentence to read: "*PCF occurs when liquid water, which can exist in narrow pores, cracks, cavities or capillaries (hereafter referred to as pores) below ambient water saturation, freezes*." on page 2 lines 8-9.

• (2, 12) I think that either "concave" should be curved, or the sign convention defined. I believe the equation is general up to the choice of sign convention for the radius of curvature.

For clarity we have now reformulated the sentence to state "*negative or concave curvature*", on page 2, line 9.

• (2, Eq. 2) To me Eq. 2 represents an amalgamation of the critical cluster size of an ice germ in the vapor and liquid phases. Given the discussion I understand the critical radius for an ice germ in the liquid phase should be presented, and this is what is indicated by σiw I believe. Typically Si would represent a pressure ratio pv/pi , that is the actual vapor pressure divided by the equilibrium vapor pressure over ice. In the presented case should the pressure ratio not refer to the pressure across the interface of the ice germ in liquid, i.e., pw/pi? See Marcolli 2 Eq. 11.

Thank you for pointing this out, indeed the ratio should be that of water and ice. The equation has been updated accordingly. The description of Eq. 2 now reads: "*where σ_{iw} is the interfacial energy between the ice and water interface, v_{ice} is the approximate volume of bulk ice, and $\frac{p_w}{p_i}$ is the ratio of the equilibrium vapour pressures over water and ice*." on page 2 lines 29-30.

• (3,3) The assumption of t = 0.38 nm from Schrieber et al., 2001 might warrant an additional comment. It is important to note that this value will certainly be temperature dependent, and that given the changes in surface functional group it might vary between tested samples. Given that as is it represents a sizable fraction of the pore diameter such potential changes might be important. Fig.7 from Bartels-Rausch et al. 3 is a good summary of the variation over a range of temperatures that such a surface layer can take on – at the free surface, with respect to theory, measurements, and modeling. That said the pore surface is something different, beginning as a liquid/solid(pore material) interface, and when ice forms any 'quasi-liquid' layer would be a function of the specific intermolecular interactions of that system. It might be more simple to state that the expected thickness of such a layer at such temperatures would likely be of order 1 molecular layer (≈ 2.5A for water).

Indeed, the width of the quasi-liquid layer on flat surfaces varies with temperature and with surface functional groups, and the same is the case for the quasi-liquid layer within pores. Yet, the exact width of the quasi-liquid layer is uncertain and a parameterization as a function of temperature out of scope. Schreiber et al. (2001) determined a value of t = 0.38 nm by fitting measured melting point depressions to a modified Gibbs-Thomson equation. Since the temperature range (223 - 263 K) and pore diameters (3 – 12 nm) investigated in Schreiber et al, (2001) are the same as in this study, t = 0.38 nm seems appropriate for the experiments carried out in this study. Furthermore, the assumption of t = 0.38 nm leads to a good agreement with our own results as can be seen from the DSC measurements and with melting point depressions compiled from literature in Marcolli (2014). We have now added: *"The width*

of the quasi-liquid layer has been shown to depend on temperature and surface chemistry but the exact thickness of the layer varies greatly between different observational techniques and MD studies (Bartels-Rausch et al., 2014). Nevertheless, the thickness of the quasi-liquid layer can be parameterized by fitting the measured melting point depressions of ice in pores to a modified version of the Gibbs-Thomson equation and has been shown to vary between 1 and 2 monolayers thick for the pore diameters and across the temperature range investigated in this study (Findenegg et al., 2008; Jähnert et al., 2008; Marcolli, 2014; Schreiber et al., 2001; Wang et al., 2019)*. When accounting for the quasi-liquid layer thickness, assumed as t = 0.38 nm (Schreiber et al., 2001), the diameter of a pore capable of hosting ice (D_p) can be expressed as:…*" to the discussion on page 3 lines 1-9.

As an additional comment related to this and Eq. (3), is that any 'quasi-liquid' layer thickness t would be an equilibrium phenomenon, and it is not self-evident that it should be considered as a limit to the volume available for nucleation, which is fundamentally non-equilibrium. In fact the heterogeneity at the pore surface might help to initiate nucleation even if the relaxed, low-energy state of the system would prefer disorder.

Remember taken from the point of view of pore ice the layer closest to the pore wall may be disordered or 'quasi-liquid' but taken from the viewpoint of pore water the surface layer may exhibit enhanced order. That might stimulate nucleation in analogy to what is noted (22, 25-27) in the 9.0M2 particles which the authors say contain ice nucleation sites even at higher temperatures.

The water in the quasi-liquid layer is not available for incorporation into the critical ice embryo as it is bound to the pore surface (i.e. due to the interaction with the pore surface, it is at a lower chemical potential than the bulk of the pore water). Since the interaction with the pore wall depends on the functionalization of the pore surface, the thickness and the structure of the quasi-liquid layer indeed depends on the pore surface properties and it also may be structured in a way suitable for ice formation, i.e. it may act as an ice-nucleating surface inducing heterogeneous ice nucleation. Within the framework of CNT, this is described by amending the Gibbs free energy barrier of nucleation with a term that depends on the contact angle between the ice embryo and the pore surface, implying a spherical-cap-shaped embryo instead of a sphere. However, heterogeneous ice nucleation would still be limited by the width of the pore and therefore, the pore diameter would still need to be wide enough for bulk ice to fit inside the pore. For the pore diameters where heterogeneous freezing can occur without being impeded by the critical pore diameters (9.1H2 and 9.0M2) the ordering/disordering of the quasi-liquid layer may be responsible for the observed freezing. We discuss this on page 25 starting on line 10.

• (3, 5-10) I find the discussion of water saturation in and out of the pore confusing, also see my comment on Eq. 2 above. My basic understanding is that within the pore everything is occurring in condensed liquid?

We have reformulated the paragraph for clarity and it now reads: "*Based on CNT, the ice growing out of the pore needs to be supercritical with respect to the vapour phase. The energy barrier for nucleation in the vapour phase is significantly higher than that in water. This increase in energy barrier comes from the need to replace σ_{iw} with the interfacial energy between ice and vapour (σ_{iv}) in Eq. 2,*

which is approximately a factor of 4.8 larger than σ_{iw} at 236 K (Cooper, 1974; Ickes et al., 2015; Ketcham and Hobbs, 1969). Additionally, as the ice growing out of the pore experiences an environment that is subsaturated with respect to water, $\frac{p_w}{p_i}$ in Eq. 2 must be replaced by the ice saturation ratio (S_i), which is smaller than $\frac{p_w}{p_i}$. Therefore, the critical radius for ice growth out of the pore is much larger than that of the critical radius in the pore necessitating a substantial increase in the ice saturation ratio (S_i) for ice to be able to grow out of a pore…" on page 3 lines 12-19.

• (4,17) For the uninitiated a "Teflon bomb" is unfamiliar terminology.

Thank you for pointing this out. We have now revised the terminology to state: "*a Teflon lined acid digestion vessel*" on page 4, lines 14-15

• (4,25) Here and throughout the manuscript the authors should be careful with how they refer to contact angle. "these were observed to change contact angle with ageing in air" (Note aging misspelled).

Thank you for pointing this out. We have now reformulated the sentence to state: "*We will focus on ice nucleation experiments with particles functionalized with trimethyl and hydroxyl groups rather than just calcined ones, as their contact angle with water was observed to change with aging in air (Muster et al., 2001)*." on page 5 lines 6-8.

I believe they intend to say that the water contact angle with these was observed to change after aging in air? In any case the authors should review all uses of contact angle, or use a defined 'water contact angle' throughout, to make sure the use of contact angle is correct and consistent throughout the text.

We have now revised the manuscript to clarify that contact angle refers to the water contact angle.

As a follow-up question, was the changing water contact angle with calcinated particles systematic with aging as a function of any monitored variable, like RH? If so these types of particles might offer another useful experimental system.

Unfortunately, the storage humidity was not monitored over the period during which we performed experiments with calcined particles. Therefore, it is not possible to quantify the time or conditions that led to observed changes in the water contact angle of the particles. As such, those experiments are not included in the present manuscript. Nevertheless, this may be a valid approach to investigate the impact of water contact angles on the PCF mechanism for future studies.

• (5,2) "filtered off" What is meant here?

We have clarified the text to read: "… *before the suspension was filtered and washed*…" on page 5 line 16

• (5,12) I think either BET should not appear as an acronym at first use, or perhaps it is enough to make it slightly more descriptive, for example: applying BET adsorption theory

Thanks, we have now changed the text to read: "… *and applying the Brunauer, Emmett and Teller (BET) gas adsorption theory*…" on page 6 lines 7-8

• (6,14) p/p0 could be better explained. It appears related to a comment below (13, 6), but the connection could be made more clear.

To connect p/p_0 to RH_w we have changed the text to read: "…*p/p_0 is the water saturation ratio or $RH_w/100$*." On page 7 line 2. Additionally, we have clarified the p/p_0 value used when calculating the water contact angle of the pores by stating: "*When deriving θ, p/p_0 is identified as the saturation ratio where the pore condensation step of the DVS measurement is the steepest*." on page 7 line 10-11.

• (7,13) Were any other sized particles bigger or smaller than 400 nm tested? Why or why not? It would be nice to rule out any effect of particle size when considering the results.

The particles were synthesized to be 400 nm in order for the observed differences in ice nucleation ability to be directly attributable to differences in pore diameters and water contact angles of the particles rather than the particle size. I. e. it was a means to eliminate one variable. The effect of particle size might be an additional parameter to be tested in future studies.

• (7,27) Contact angle again. Here it is not the pores contact angle, but I think water's contact angle with or within the pores.

In accordance with the previous comment on contact angle, we have now updated the manuscript to clearly indicate that the water contact angle with the pore or particle surface is meant.

• (13,6) See also comment above with regard to how the RH of the first sorption cycle is used. As a general comment, I would expect the hysteresis between adsorption and desorption should offer an additional verification of the pore size that is presented earlier in §3.1. It seems that the magnitude of the hysteresis, if the RH ramping is done is a quasi-steady state manner, should be directly related to the stability of the liquid in the pores. Was an effort made to use the information in this manner, or do I miss a complicating factor? Finally, have the author's considered how to propagate the uncertainty to bound the uncertainty in contact angle as derived from use with Eq. 7?

The observed hysteresis between adsorption and desorption isotherms can indeed be used to infer the pore shape and pore size as long as the pores maintain a constant water contact angle. However, the change in adsorption and desorption isotherms in the subsequent cycles indicates that the water contact angle of the pores changes with initial exposure to increasing humidity. We therefore use nitrogen adsorption to determine the pore diameters and the initial water vapour sorption cycle to infer contact angles using the pore diameters determined from nitrogen adsorption. The water uptake during the first water vapour sorption cycle is most representative of the contact angle relevant for water uptake in our ice nucleation experiments as the experiments are the first instance that the pores are exposed to high concentrations of water vapor.

• (Figure 4) The upper axes are missing a unit label. I am impressed by the agreement between the observed heat flow and the predicted critical pore diameter from the bulk physical model.

Thank you, we have now added "*nm*" to the upper axis of this figure. Indeed, it shows that the values used to constrain the interfacial tension from Murray et al., (2010) and Zobrist et al., (2007) are working well. Additionally, it corroborates that assuming a quasi-liquid layer of 0.38 nm is appropriate.

• (16,6) Why is AF 0.05 chosen? Is this simply an experimental choice of the minimum AF at which nucleation can be observed? A clear explanation would be useful, especially given that in many nucleation studies of controlled materials different AF may be chosen for plotting.

Thank you for pointing this out. The *AF* of 0.05 was chosen due to the distribution in pore sizes and functional groups on the particles. Using a lower AF to represent the average freezing RH of the porous particles, may lead to the misinterpretation of the freezing results due to the presence of unique particle features that may exist on a few of the particles. We have now added the following to clarify this choice in the main text: "*An AF of 0.05 was chosen as best representing the average freezing RH of the porous particles*." starting on page 17 line 10.

• (16, 23) Although the Skrotzki paper is directed to cirrus clouds, many such uptake measurements have been undertaken over the years and are notoriously difficult to parse. Furthermore the values in the literature vary over orders of magnitude. Direct studies of molecular uptake are presented in Kong et al. 4 as well as a review and comparison with measurement and simulation studies (including the Skrotzki paper). However, perhaps for these studies it must also be considered that the changes in functional groups that are utilized also likely lead to changes in uptake coefficient. This is clear from the adosorption/desorption isotherms in Fig. 3. It has also been previously documented that even thin surface coatings can significantly affect uptake.5,6 I would recommend some reference to this body of work be included.

Since pores are closely spaced in our particles, pore openings make up a relevant fraction of the particle surface. We therefore assume that ice grows on the ice-covered part of the particle surface, for which the accommodation coefficient on ice is relevant. Molecular dynamic simulations presented in David et al. (2019), which show that ice rapidly covers the entire particle surface, further support this assumption.

We revised the discussion of the delayed freezing onset RH following a comment of reviewer #1, who pointed out that an accommodation coefficient of 0.1 is at the lower limit of experimentally determined values. We now widened up the discussion on page 18 lines 20-29 to include all potential reasons.

• (Fig. 7 caption) As in Fig. 6 caption it should be stated that points correspond to AF 0.05 condition.

Thank you for pointing this out, we have now updated the caption accordingly.

• (Fig. 8) This figure seems a bit out of place and is of limited use in the explanation here. Perhaps it could be introduced earlier in the particle characterization section and returned to here?

We have now moved to the beginning of the manuscript (new Fig.1) and introduce it on page 4 lines 6 and 20-21 by stating: "*The MCM-41 (see Fig. 1a and b) particles were synthesized following Beck et al., (1992),…" and "To obtain larger pore diameters (~9 nm), SBA-15 particles (see Fig. 1c and d) were synthesized similarly to Linton et al., (2009b) where Pluronic® P104 (1.25 g, BASF) was*…".

• (25, 26) It might be a bit strong to say that parameterizations should be based on PCF. Perhaps, should include?

We have reformulated the sentence to state: "… *parametrizations should include the PCF mechanism below the HFT*…" on page 27 lines 5-6.

• (25, 26) The final sentence links this work to understanding anthropogenic emissions, but this is really the first mention of such emissions up to this point. Are these particles particularly analogous to any known anthropogenic emission? If the link is not strong I think this point can be left out, there are of course many reasons to better understand the effects of porosity and geometry on freezing.

We have now added reference to soot particles as an example of anthropogenic emissions, which have recently been shown to nucleate ice following PCF to text as follows: *"…, such as soot, which has been shown to nucleate ice in accordance with PCF (Mahrt et al., 2018, 2020b, 2020a; Nichman et al., 2019)*,…" on page 25 lines 13-15.

Summary: I have enjoyed reading the submitted manuscript. I reiterate that I think it could benefit from an improved clarity with regard to the concrete conclusions the authors would like to posit. My understanding is that basic edifice of PCF which rests on the inverse Kelvin equation does a good job of predicting the experimental observations if some of the asserted assumptions are valid. It appears that as with many systems a complete understanding of the data would involve a much more comprehensive picture of the intermolecular interactions specific to each system. The measurements rely both on ice nucleation and crystal growth to a detectible size, thus many details related to both the ice initiation and macroscopic state are convoluted. Such complexities are intrinsic in many experiments, yet I still feel this study brings the community a step forward. However, it appears the open question remains as to how this might be utilized and tested in a messier real atmospheric aerosol scenario.

We would like to thank the reviewer for commending the efforts made in this study to disentangle the complex relationship between pore size and ability of pores to uptake water within the PCF framework. Indeed, it is our intention that this study lays the foundation for future studies to further quantify the PCF mechanism for its application in real atmosphere particles thus improving the representation in cloud models via ice nucleation parametrizations.

Reviewer References:

[1] Vali, G., DeMott, P. J., Mohler, O., and Whale, T. F. (2015). Technical note: A proposal for ice ¨ nucleation terminology. Atmospheric Chemistry and Physics, 15(18):10263–10270.

[2] Marcolli, C. (2014). Deposition nucleation viewed as homogeneous or immersion freezing in pores and cavities. Atmospheric Chemistry and Physics, 14(4):2071–2104.

[3] Bartels-Rausch, T., Jacobi, H.-W., Kahan, T. F., Thomas, J. L., Thomson, E. S., Abbatt, J. P. D., Ammann, M., Blackford, J. R., Bluhm, H., Boxe, C., Domine, F., Frey, M. M., Gladich, I., Guzman, ´ M. I., Heger, D., Huthwelker, T., Klan, P., Kuhs, W. F., Kuo, M. H., Maus, S., Moussa, S. G., McNeill, ´ V. F., Newberg, J. T., Pettersson, J. B. C., Roeselova, M., and Sodeau, J. R. (2014). A review of air– ´ ice chemical and physical interactions (AICI): liquids, quasi-liquids, and solids in snow. Atmospheric Chemistry and Physics, 14(3):1587–1633.

[4] Kong, X., Papagiannakopoulos, P., Thomson, E. S., Markovic, N., and Pettersson, J. B. C. (2014a). ´ Water accommodation and desorption kinetics on ice. The Journal of Physical Chemistry A, 118(22):3973–3979.

[5] Kong, X., Thomson, E. S., Papagiannakopoulos, P., Johansson, S. M., and Pettersson, J. B. C. (2014b). Water accommodation on ice and organic surfaces: Insights from environmental molecular beam experiments. The Journal of Physical Chemistry B, 118(47):13378–13386.

[6] Thomson, E. S., Kong, X., Markovic, N., Papagiannakopoulos, P., and Pettersson, J. B. C. (2013). ´ Collision dynamics and uptake of water on alcohol-covered ice. Atmospheric Chemistry and Physics, 13(4):2223–2233.

Author References:

Bartels-Rausch, T., Jacobi, H.-W., Kahan, T. F., Thomas, J. L., Thomson, E. S., Abbatt, J. P. D., Ammann, M., Blackford, J. R., Bluhm, H., Boxe, C., Domine, F., Frey, M. M., Gladich, I., Guzmán, M. I., Heger, D., Huthwelker, T., Klán, P., Kuhs, W. F., Kuo, M. H., Maus, S., Moussa, S. G., McNeill, V. F., Newberg, J. T., Pettersson, J. B. C., Roeselová, M. and Sodeau, J. R.: A review of air–ice chemical and physical interactions (AICI): liquids, quasi-liquids, and solids in snow, Atmospheric Chem. Phys., 14(3), 1587–1633, doi:https://doi.org/10.5194/acp-14-1587-2014, 2014.

Beck, J. S., Vartuli, J. C., Roth, W. J., Leonowicz, M. E., Kresge, C. T., Schmitt, K. D., Chu, C. T. W., Olson, D. H., Sheppard, E. W. and McCullen, S. B.: A new family of mesoporous molecular sieves prepared with liquid crystal templates, J. Am. Chem. Soc., 114(27), 10834–10843, 1992.

Cooper, W. A.: A Possible Mechanism for Contact Nucleation, J. Atmospheric Sci., 31(7), 1832–1837, doi:10.1175/1520-0469(1974)031<1832:APMFCN>2.0.CO;2, 1974.

Findenegg, G. H., Jähnert, S., Akcakayiran, D. and Schreiber, A.: Freezing and Melting of Water Confined in Silica Nanopores, ChemPhysChem, 9(18), 2651–2659, doi:10.1002/cphc.200800616, 2008.

Fletcher, N. H.: Active Sites and Ice Crystal Nucleation, J. Atmospheric Sci., 26(6), 1266–1271, doi:10.1175/1520-0469(1969)026<1266:ASAICN>2.0.CO;2, 1969.

Ickes, L., Welti, A., Hoose, C. and Lohmann, U.: Classical nucleation theory of homogeneous freezing of water: thermodynamic and kinetic parameters, Phys. Chem. Chem. Phys. PCCP, 17(8), 5514–5537, doi:10.1039/c4cp04184d, 2015.

Jähnert, S., Vaca Chávez, F., Schaumann, G. E., Schreiber, A., Schönhoff, M. and Findenegg, G. H.: Melting and freezing of water in cylindrical silica nanopores, Phys. Chem. Chem. Phys., 10(39), 6039, doi:10.1039/b809438c, 2008.

Kaufmann, L., Marcolli, C., Luo, B. and Peter, T.: Refreeze experiments with water droplets containing different types of ice nuclei interpreted by classical nucleation theory, Atmos Chem Phys, 17(5), 3525–3552, doi:10.5194/acp-17-3525-2017, 2017.

Ketcham, W. M. and Hobbs, P. V.: An experimental determination of the surface energies of ice, Philos. Mag., 19(162), 1161–1173, doi:10.1080/14786436908228641, 1969.

Kiselev, A., Bachmann, F., Pedevilla, P., Cox, S. J., Michaelides, A., Gerthsen, D. and Leisner, T.: Active sites in heterogeneous ice nucleation—the example of K-rich feldspars, Science, 355(6323), 367–371, doi:10.1126/science.aai8034, 2017.

Linton, P., Hernandez-Garrido, J.-C., Midgley, P. A., Wennerström, H. and Alfredsson, V.: Morphology of SBA-15-directed by association processes and surface energies, Phys. Chem. Chem. Phys., 11(46), 10973–10982, doi:10.1039/B913755F, 2009.

Mahrt, F., Marcolli, C., David, R. O., Grönquist, P., Meier, B., J, E., Lohmann, U. and Kanji, Z. A.: Ice nucleation abilities of soot particles determined with the Horizontal Ice Nucleation Chamber, Atmospheric Chem. Phys. Discuss., 1–41, doi:https://doi.org/10.5194/acp-2018-557, 2018.

Mahrt, F., Alpert, P. A., Dou, J., Grönquist, P., Arroyo, P. C., Ammann, M., Lohmann, U. and Kanji, Z. A.: Aging induced changes in ice nucleation activity of combustion aerosol as determined by near edge X-ray absorption fine structure (NEXAFS) spectroscopy, Environ. Sci. Process. Impacts, 22(4), 895–907, doi:10.1039/C9EM00525K, 2020a.

Mahrt, F., Kilchhofer, K., Marcolli, C., Grönquist, P., David, R. O., Rösch, M., Lohmann, U. and Kanji, Z. A.: The Impact of Cloud Processing on the Ice Nucleation Abilities of Soot Particles at Cirrus Temperatures, J. Geophys. Res. Atmospheres, 125(3), e2019JD030922, doi:10.1029/2019JD030922, 2020b.

Marcolli, C.: Deposition nucleation viewed as homogeneous or immersion freezing in pores and cavities, Atmos Chem Phys, 14(4), 2071–2104, doi:10.5194/acp-14-2071-2014, 2014.

Murray, B. J., L. Broadley, S., W. Wilson, T., J. Bull, S., H. Wills, R., K. Christenson, H. and J. Murray, E.: Kinetics of the homogeneous freezing of water, Phys. Chem. Chem. Phys., 12(35), 10380–10387, doi:10.1039/C003297B, 2010.

Muster, T. H., Prestidge, C. A. and Hayes, R. A.: Water adsorption kinetics and contact angles of silica particles, Colloids Surf. Physicochem. Eng. Asp., 176(2), 253–266, 2001.

Nichman, L., Wolf, M., Davidovits, P., Onasch, T. B., Zhang, Y., Worsnop, D. R., Bhandari, J., Mazzoleni, C. and Cziczo, D. J.: Laboratory study of the heterogeneous ice nucleation on black-carbon-containing aerosol, Atmospheric Chem. Phys., 19(19), 12175–12194, doi:https://doi.org/10.5194/acp-19-12175-2019, 2019.

Schreiber, A., Ketelsen, I. and Findenegg, G. H.: Melting and freezing of water in ordered mesoporous silica materials, Phys. Chem. Chem. Phys., 3(7), 1185–1195, doi:10.1039/B010086M, 2001.

Vali, G., DeMott, P. J., Möhler, O. and Whale, T. F.: Technical Note: A proposal for ice nucleation terminology, Atmospheric Chem. Phys., 15(18), 10263–10270, doi:10.5194/acp-15-10263-2015, 2015.

Wang, J., Xue, H., Zhou, B., Yao, Y.-F. and Hansen, E. W.: Interfacial water in mesopores and its implications to the surface features – A solid state NMR study, Appl. Surf. Sci., 484, 1154–1160, doi:10.1016/j.apsusc.2019.04.095, 2019.

Zobrist, B., Koop, T., Luo, B. P., Marcolli, C. and Peter, T.: Heterogeneous Ice Nucleation Rate Coefficient of Water Droplets Coated by a Nonadecanol Monolayer, J. Phys. Chem. C, 111(5), 2149–2155, doi:10.1021/jp066080w, 2007.